Chapter 9 Generalized Conforming Element for the Analysis of the Laminated Composite Plates

Song Cen
Department of Engineering Mechanics, School of Aerospace,
Tsinghua University, Beijing, 100084, China

Yu-Qiu Long
Department of Civil Engineering, School of Civil Engineering,
Tsinghua University, Beijing, 100084, China

Abstract A simple displacement-based, quadrilateral 20 DOF (5 DOF per node) bending element based on the first-order shear deformation theory (FSDT) for the analysis of the arbitrary laminated composite plates is presented in this chapter. This element is constructed by the following procedure: (1) the variation functions of the rotation and the shear strain along each side of the element are determined using the Timoshenko's beam theory; and (2) the shear strain, rotation and in-plane displacement fields in the domain of the element are then determined using the technique of improved interpolation. In fact, this is the scheme of assuming rotation and shear strain fields which has been introduced in the previous chapter. Furthermore, a simple hybrid procedure is also proposed to improve the stress solutions. The proposed element, denoted as CTMQ20, possesses the advantages of both the displacement-based and hybrid elements. Thus, excellent results for both displacements and stresses, especially for the transverse shear stresses, can be obtained.

Keywords finite element, laminated composite plate, generalized conforming, first-order shear deformation theory (FSDT), hybrid-enhanced post-processing procedure.

9.1 Introduction

During the past 40 years, high performance composite materials have been playing very important roles in the design of modern industrial products and structures for their high strength-to-weight and stiffness-to-weight ratios, and have been broadly used in many high-tech areas, such as aerospace, building, transport,

medicine, and so on. Laminated composite plate is one of the most popular structural components. Due to its particularities and complexity in construction, studies on appropriate computational theories and methods for these structures attract many researchers all the while. The finite element method provides an effective way of solution for such laminated composite plates. Various methods have been proposed based on the following theories[1]:

- The classical lamination theory based on Kirchhoff hypothesis (CLT);
- First-order shear deformation theory (FSDT);
- Higher-order shear deformation theory (HSDT);
- Layer-wise lamination theory (LLT);
- Three-dimensional (3D) elasticity.

The classical lamination theory (CLT)[2,3], which is an extension of the classical thin plate theory to laminated plates, neglects the effects due to transverse shear strains and requires C^1 continuity in displacement fields. The errors in such a theory naturally increase as the thickness-span ratio of the plate increases. The first-order shear deformation theory (FSDT) is based on the Reissner-Mindlin plate theory[4,5]. With the consideration of the transverse shear deformation effect on the plates, FSDT only requires C^0 continuity and can be used from thin to moderately thick plates. But, in FSDT, the transverse shearing strains/stresses are assumed constant through the plate thickness, which is contradictory to the zero shear stress conditions on the bounding planes of the plate. Furthermore, several fictitious shear correction coefficients must be introduced. For overcoming the limitations of FSDT, higher-order shear deformation theories (HSDT) have been proposed by some researchers. Two different approaches have been commonly employed: single-layer and multi-layer formulations. The former increases the order considered for the displacement representation in the thickness coordinates[6–10]. The latter assumes a representation formula for the displacement field in each layer, similar to that of layer-wise lamination theory[11,12]. The solutions of these higher order theories are closer to the 3D elasticity theory than those of the two former plate theories. This is especially so for very thick cases. However, the computational cost will be increased significantly.

FSDT is usually considered the best compromise between the capability for prediction and computational cost for a wide class of applications. Some methods have been proposed to solve the above-mentioned problems of the FSDT. For example, the distribution of transverse shear stresses can be evaluated by the 3D elasticity equilibrium equation[13]; Vlachoutsis[14] presented a simple procedure to calculate the shear correction factors for laminated plates and shells under cylindrical bending; Auricchio et al.[15] proposed a numerical method for solving the shear correction coefficients of arbitrary laminated composite plates; Rolfes et al.[16] presented a simple post-processing approach to obtain improved transverse shear stresses in finite element analysis based on FDST; and Rolfes et al.[17] even presented a simple and accurate post-processing method for the FSDT to calculate

the transverse normal stress, which was initially assumed to be zero. These efforts make it more convenient and reasonable to use the FSDT in practical applications.

New finite elements based on the FSDT are still proposed by many researchers[15, 18, 20]. Since many simple displacement-based elements adopt simple interpolation functions, they are unable to provide a satisfactory recovery of the transverse shear stresses. Therefore, the hybrid or mixed-hybrid elements have been playing a leading role in the analysis of the composite plates[21]. However, the formulations of the hybrid elements are more complicated than that of the displacement-based elements. Besides, shear locking may also be a problem in the construction of the laminated composite plate elements. How to develop a simple but effective model has been a problem for a long time.

In the first section of this chapter, the first-order shear deformation theory (FSDT) is introduced briefly, and a set of formulae of the Timoshenko's laminated composite beam element are also given for developing the plate element; the subsequent sections will introduce new generalized conforming laminate composite plate elements and a new hybrid-enhanced post-processing procedure for transverse stress solutions which are proposed in [22,23].

9.2 Fundamental Theory

9.2.1 First-Order Shear Deformation Theory for Laminated Composite Plates (FSDT)

With reference to Fig. 9.1, for a linear elastic arbitrary composite plate with n layers, the kinematics is governed by the mid-plane displacements u^0, v^0, the transverse displacement (deflection) w and rotations ψ_x and ψ_y:

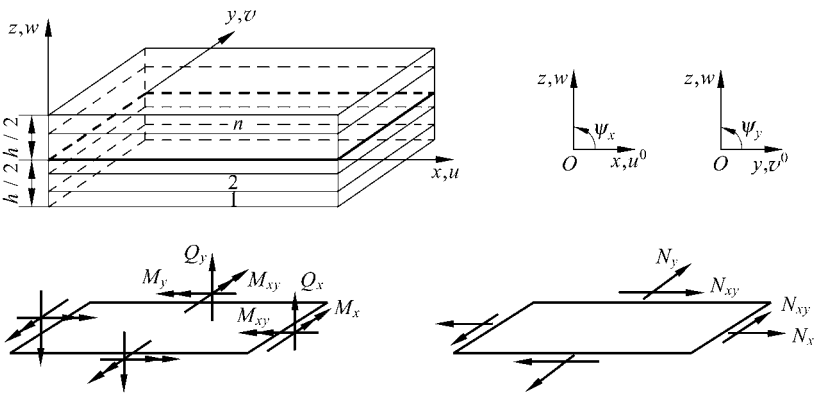

Figure 9.1 Forces and displacements at the mid-plane of a laminated composite plate

$$\begin{cases} u(x,y,z) = u^0(x,y) - z\psi_x(x,y) \\ v(x,y,z) = v^0(x,y) - z\psi_y(x,y) \\ w(x,y,z) = w(x,y) \end{cases} \tag{9-1}$$

Therefore, the total in-plane strain $\boldsymbol{\varepsilon}$ is:

$$\boldsymbol{\varepsilon} = \boldsymbol{\varepsilon}^0 + z\boldsymbol{\kappa} \tag{9-2}$$

where $\boldsymbol{\varepsilon}^0$ and $\boldsymbol{\kappa}$ are the in-plane strain of the mid-plane and the curvature vector of the plate, respectively, which are given below:

$$\boldsymbol{\varepsilon} = [\varepsilon_x \quad \varepsilon_y \quad \gamma_{xy}]^{\mathrm{T}} \tag{9-3}$$

$$\boldsymbol{\varepsilon}^0 = [\varepsilon_x^0 \quad \varepsilon_y^0 \quad \gamma_{xy}^0]^{\mathrm{T}} = \left[\frac{\partial u^0}{\partial x} \quad \frac{\partial v^0}{\partial y} \quad \frac{\partial u^0}{\partial y} + \frac{\partial v^0}{\partial x}\right]^{\mathrm{T}} \tag{9-4}$$

$$\boldsymbol{\kappa} = [\kappa_x \quad \kappa_y \quad 2\kappa_{xy}]^{\mathrm{T}} = \left[-\frac{\partial \psi_x}{\partial x} \quad -\frac{\partial \psi_y}{\partial y} \quad -\frac{\partial \psi_x}{\partial y} - \frac{\partial \psi_y}{\partial x}\right]^{\mathrm{T}} \tag{9-5}$$

The transverse shear strain vector is:

$$\boldsymbol{\gamma} = [\gamma_x \quad \gamma_y]^{\mathrm{T}} = \left[\frac{\partial w}{\partial x} - \psi_x \quad \frac{\partial w}{\partial y} - \psi_y\right]^{\mathrm{T}} \tag{9-6}$$

The stress-strain relationship with respect to the principal material axes, 1-axis and 2-axis, for the kth ($k = 1,2,\cdots,n$) layer is:

$$\begin{Bmatrix} \sigma_1 \\ \sigma_2 \\ \tau_{12} \end{Bmatrix}_k = \begin{bmatrix} Q_{11} & Q_{12} & 0 \\ Q_{12} & Q_{22} & 0 \\ 0 & 0 & Q_{66} \end{bmatrix}_k \begin{Bmatrix} \varepsilon_1 \\ \varepsilon_2 \\ \gamma_{12} \end{Bmatrix}_k \tag{9-7}$$

$$\begin{Bmatrix} \tau_{23} \\ \tau_{13} \end{Bmatrix}_k = \begin{bmatrix} Q_{44} & 0 \\ 0 & Q_{55} \end{bmatrix}_k \begin{Bmatrix} \gamma_{23} \\ \gamma_{13} \end{Bmatrix}_k \tag{9-8}$$

in which

$$\left.\begin{aligned} Q_{11k} &= \frac{E_{1k}}{1-\mu_{12k}\mu_{21k}}, \quad Q_{12k} = \frac{\mu_{21k}E_{1k}}{1-\mu_{12k}\mu_{21k}} = Q_{21k} \\ Q_{21k} &= \frac{\mu_{12k}E_{2k}}{1-\mu_{12k}\mu_{21k}}, \quad Q_{22k} = \frac{E_{2k}}{1-\mu_{12k}\mu_{21k}} \\ Q_{66k} &= G_{12k}, \quad Q_{44k} = G_{23k}, \quad Q_{55k} = G_{13k} \end{aligned}\right\} \tag{9-9}$$

where σ_{1k}, σ_{2k}, τ_{12k}, τ_{23k} and τ_{13k} are the two principal direct stresses, the in-plane shear stresses and the transverse shear stresses of the kth layer, respectively; ε_{1k}, ε_{2k}, γ_{12k}, γ_{23k} and γ_{13k} are the corresponding strains; E_{1k} and E_{2k} are the Young's modulus in the direction of the fibres (1-axis) and transverse to the fibres (2-axis), respectively; G_{12k} is the in-plane shear modulus, G_{23k} and G_{13k} are the transverse shear modulus, μ_{12k} is the major Poisson's ratio, and $\mu_{21k} = \mu_{12k}\dfrac{E_{2k}}{E_{1k}}$.

Thus, the stress-strain relationship with respect to x-axis and y-axis for the kth ($k = 1,2,\cdots,n$) layer is

$$\boldsymbol{\sigma}_k = \begin{Bmatrix} \sigma_x \\ \sigma_y \\ \tau_{xy} \end{Bmatrix}_k = \begin{bmatrix} \bar{Q}_{11} & \bar{Q}_{12} & \bar{Q}_{16} \\ \bar{Q}_{12} & \bar{Q}_{22} & \bar{Q}_{26} \\ \bar{Q}_{16} & \bar{Q}_{26} & \bar{Q}_{66} \end{bmatrix}_k \begin{Bmatrix} \varepsilon_x \\ \varepsilon_y \\ \gamma_{xy} \end{Bmatrix} = \bar{\boldsymbol{Q}}_k \boldsymbol{\varepsilon} \tag{9-10}$$

$$\boldsymbol{\tau}_{zk} = \begin{Bmatrix} \tau_{xz} \\ \tau_{yz} \end{Bmatrix}_k = \begin{bmatrix} k_1^2 \bar{Q}_{55} & k_1 k_2 \bar{Q}_{45} \\ k_1 k_2 \bar{Q}_{45} & k_2^2 \bar{Q}_{44} \end{bmatrix}_k \begin{Bmatrix} \gamma_{xz} \\ \gamma_{yz} \end{Bmatrix} = \bar{\boldsymbol{C}}_{sk} \boldsymbol{\gamma} \tag{9-11}$$

in which k_1^2, $k_1 k_2$ and k_2^2 are the shear correction coefficients;

$$\begin{cases} \bar{Q}_{11k} = Q_{11k} l_k^4 + 2(Q_{12k} + 2Q_{66k}) l_k^2 m_k^2 + Q_{22k} m_k^4 \\ \bar{Q}_{12k} = (Q_{11k} + Q_{22k} - 4Q_{66k}) l_k^2 m_k^2 + Q_{12k}(l_k^4 + m_k^4) \\ \bar{Q}_{22k} = Q_{11k} m_k^4 + 2(Q_{12k} + 2Q_{66k}) l_k^2 m_k^2 + Q_{22k} l_k^4 \\ \bar{Q}_{16k} = (Q_{11k} - Q_{12k} - 2Q_{66k}) l_k^3 m_k + (Q_{12k} - Q_{22k} + 2Q_{66k}) l_k m_k^3 \\ \bar{Q}_{26k} = (Q_{11k} - Q_{12k} - 2Q_{66k}) l_k m_k^3 + (Q_{12k} - Q_{22k} + 2Q_{66k}) l_k^3 m_k \\ \bar{Q}_{66k} = (Q_{11k} + Q_{22k} - 2Q_{12k} - 2Q_{66k}) l_k^2 m_k^2 + Q_{66k}(l_k^4 + m_k^4) \\ \bar{Q}_{44k} = Q_{44k} l_k^2 + Q_{55k} m_k^2 \\ \bar{Q}_{45k} = (Q_{55k} - Q_{44k}) l_k m_k \\ \bar{Q}_{55k} = Q_{44k} m_k^2 + Q_{55k} l_k^2 \end{cases} \tag{9-12}$$

$$l_k = \cos\theta_k, \quad m_k = \sin\theta_k \tag{9-13}$$

θ_k is the angle between the x-axis and the fiber direction 1-axis of the kth layer.

The constitutive relationship of the laminated composite plate can be expressed as:

$$\boldsymbol{\sigma}_{\mathrm{p}} = \begin{Bmatrix} \boldsymbol{N} \\ \boldsymbol{M} \end{Bmatrix} = \begin{bmatrix} \boldsymbol{A} & \boldsymbol{B} \\ \boldsymbol{B} & \boldsymbol{D} \end{bmatrix} \begin{Bmatrix} \boldsymbol{\varepsilon}^0 \\ \boldsymbol{\kappa} \end{Bmatrix} = \boldsymbol{C}_{\mathrm{p}} \boldsymbol{\varepsilon}_{\mathrm{p}} \tag{9-14}$$

$$\boldsymbol{Q} = \boldsymbol{C}_{\mathrm{s}} \boldsymbol{\gamma} \tag{9-15}$$

where $\boldsymbol{N}$ is the membrane force vector of the mid-plane; $\boldsymbol{M}$ is the bending

moment vector; $\boldsymbol{Q}$ is the transverse shear force vector; $\boldsymbol{A}$ is the extensional stiffness; $\boldsymbol{B}$ is the bending-extension stiffness; $\boldsymbol{D}$ is the bending stiffness; $\boldsymbol{C}_{\mathrm{s}}$ is the shear stiffness. These matrices can be expressed in the following forms:

$$\boldsymbol{N}=[N_x \quad N_y \quad N_{xy}]^{\mathrm{T}}, \quad \boldsymbol{M}=[M_x \quad M_y \quad M_{xy}]^{\mathrm{T}} \tag{9-16}$$

$$\boldsymbol{Q}=[Q_x \quad Q_y]^{\mathrm{T}} \tag{9-17}$$

$$\boldsymbol{A}=\begin{bmatrix} A_{11} & A_{12} & A_{16} \\ A_{12} & A_{22} & A_{26} \\ A_{16} & A_{26} & A_{66} \end{bmatrix}, \quad \boldsymbol{B}=\begin{bmatrix} B_{11} & B_{12} & B_{16} \\ B_{12} & B_{22} & B_{26} \\ B_{16} & B_{26} & B_{66} \end{bmatrix}, \quad \boldsymbol{D}=\begin{bmatrix} D_{11} & D_{12} & D_{16} \\ D_{12} & D_{22} & D_{26} \\ D_{16} & D_{26} & D_{66} \end{bmatrix} \tag{9-18}$$

$$\boldsymbol{C}_{\mathrm{s}}=\begin{bmatrix} C_{55} & C_{45} \\ C_{45} & C_{44} \end{bmatrix}=\begin{bmatrix} k_1^2 C_{55}^0 & k_1 k_2 C_{45}^0 \\ k_1 k_2 C_{45}^0 & k_2^2 C_{44}^0 \end{bmatrix} \tag{9-19}$$

$$\left.\begin{aligned} A_{ij} &= \int_{-h/2}^{h/2} \bar{Q}_{ij}\mathrm{d}z = \sum_{k=1}^{n} \bar{Q}_{ijk}(h_k - h_{k-1}) \\ B_{ij} &= \int_{-h/2}^{h/2} \bar{Q}_{ij} z\mathrm{d}z = \frac{1}{2}\sum_{k=1}^{n} \bar{Q}_{ijk}(h_k^2 - h_{k-1}^2) \\ D_{ij} &= \int_{-h/2}^{h/2} \bar{Q}_{ij} z^2\mathrm{d}z = \frac{1}{3}\sum_{k=1}^{n} \bar{Q}_{ijk}(h_k^3 - h_{k-1}^3) \end{aligned}\right\} \quad (i,j=1,2,6) \tag{9-20}$$

$$C_{ij}^0 = \int_{-h/2}^{h/2} \bar{Q}_{ij}\mathrm{d}z = \sum_{k=1}^{n} \bar{Q}_{ijk}(h_k - h_{k-1}) \quad (i,j=4,5) \tag{9-21}$$

where h_k is the z-coordinate of the upper surface for the kth layer, $h_0=-h/2$ and $h_n=h/2$, h is the thickness of the plate.

The inverse relations of Eqs. (9-14) and (9-15) are as follows:

$$\boldsymbol{\varepsilon}_{\mathrm{p}}=\boldsymbol{S}_{\mathrm{p}}\boldsymbol{\sigma}_{\mathrm{p}} \tag{9-22}$$

$$\boldsymbol{\gamma}=\boldsymbol{S}_{\mathrm{s}}\boldsymbol{Q} \tag{9-23}$$

where

$$\boldsymbol{S}_{\mathrm{p}}=\boldsymbol{C}_{\mathrm{p}}^{-1}=\begin{bmatrix} \boldsymbol{A} & \boldsymbol{B} \\ \boldsymbol{B} & \boldsymbol{D} \end{bmatrix}^{-1}=\begin{bmatrix} \boldsymbol{S}_{e3\times6} \\ \boldsymbol{S}_{b3\times6} \end{bmatrix} \tag{9-24}$$

$$\boldsymbol{S}_{\mathrm{s}}=\boldsymbol{C}_{\mathrm{s}}^{-1} \tag{9-25}$$

Substitution of Eq. (9-2) into Eq. (9-10) yields:

$$\boldsymbol{\sigma}_k = \bar{\boldsymbol{Q}}_k(\boldsymbol{\varepsilon}^0 + z\boldsymbol{\kappa}) \tag{9-26}$$

Then, substitution of Eqs. (9-14) and (9-24) into the above equation yields:

$$\boldsymbol{\sigma}_k = \bar{\boldsymbol{Q}}_k(\boldsymbol{S}_e + z\boldsymbol{S}_b)\boldsymbol{\sigma}_{\mathrm{p}} \tag{9-27}$$

9.2.2 Locking-free Timoshenko Laminated Composite Beam Element

As shown in Fig. 9.2, for a Timoshenko laminated composite beam element, the formulas of deflection w, rotation ψ and shear strain γ for the element are still given by Eqs. (8-99) and (8-100), in which D and C should be replaced by the following D_d and C_d:

$$D_d = \frac{1}{3}\sum_{k=1}^{n}(\bar{Q}_{11k})_{\bar{ij}}(h_k^3 - h_{k-1}^3) \tag{9-28}$$

with

$$(\bar{Q}_{11k})_{\bar{ij}} = Q_{11k}l_{k\bar{ij}}^4 + 2(Q_{12k} + 2Q_{66k})l_{k\bar{ij}}^2 m_{k\bar{ij}}^2 + Q_{22k}m_{k\bar{ij}}^4 \tag{9-29}$$

$$l_{k\bar{ij}} = \cos(\theta_k - \theta_{\bar{ij}}), \quad m_{k\bar{ij}} = \sin(\theta_k - \theta_{\bar{ij}}) \tag{9-30}$$

where $\theta_{\bar{ij}}$ is the angle between the x-axis and the beam (see Fig. 9.2). $\theta_k - \theta_{\bar{ij}}$ is the angle between the beam $\bar{ij}$ and the 1-axis of the kth layer.

$$C_d = (k_1^2 l_{\bar{ij}}^2 + k_2^2 m_{\bar{ij}}^2)\sum_{k=1}^{n}(\bar{Q}_{55k})_{\bar{ij}}(h_k - h_{k-1}) \tag{9-31}$$

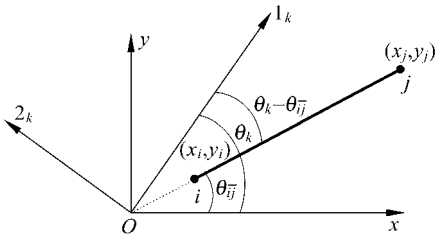

Figure 9.2 The orientation of a Timoshenko beam element $\bar{ij}$ in the coordinate system xOy and the material principal coordinate system $O12$ of the kth layer

with

$$(\bar{Q}_{55k})_{\bar{ij}} = Q_{55k} l_{\bar{ij}}^2 + Q_{44k} m_{\bar{ij}}^2 \tag{9-32}$$

$$l_{\bar{ij}} = \cos\theta_{\bar{ij}}, \quad m_{\bar{ij}} = \sin\theta_{\bar{ij}} \tag{9-33}$$

9.3 New Element CTMQ20 for the Analysis of Laminated Composite Plates

To construct the new laminated composite plate elements by using the generalized conforming thick-thin plate elements is a new scheme proposed recently. In references [22] and [23], two new models based on FSDT, TMQ20 and CTMQ20, have been successfully developed. They are constructed by adding the bilinear in-plane displacement field to the formulations of the quadrilateral thick-thin elements TMQ[24] and ARS-Q12[25], respectively. This section will introduce the construction procedure of the element CTMQ20 proposed in [23].

Consider the quadrilateral arbitrary laminated composite plate element shown in Fig. 9.3. The element nodal displacement vector is:

$$\left.\begin{aligned} \boldsymbol{q}^e &= [\boldsymbol{q}_1 \quad \boldsymbol{q}_2 \quad \boldsymbol{q}_3 \quad \boldsymbol{q}_4]^{\mathrm{T}} \\ \boldsymbol{q}_i &= [u_i \quad v_i \quad w_i \quad \psi_{xi} \quad \psi_{yi}]^{\mathrm{T}} \quad (i = 1,2,3,4) \end{aligned}\right\} \tag{9-34}$$

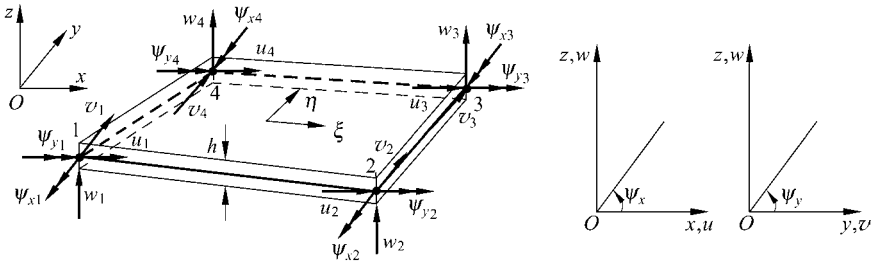

Figure 9.3 A 4-node quadrilateral laminated composite plate element

9.3.1 Interpolation Formulas for the Shear Strain Fields

1. Shear strain along the element sides

According to Eq. (8-99c), the transverse shear strain along the tangential direction (s-direction) of each side can be written as:

$$\left.\begin{aligned}
\gamma_{s1} &= -\frac{\delta_1}{d_1}[2(w_2 - w_3) + (c_1\psi_{x2} - b_1\psi_{y2}) + (c_1\psi_{x3} - b_1\psi_{y3})] \\
\gamma_{s2} &= -\frac{\delta_2}{d_2}[2(w_3 - w_4) + (c_2\psi_{x3} - b_2\psi_{y3}) + (c_2\psi_{x4} - b_2\psi_{y4})] \\
\gamma_{s3} &= -\frac{\delta_3}{d_3}[2(w_4 - w_1) + (c_3\psi_{x4} - b_3\psi_{y4}) + (c_3\psi_{x1} - b_3\psi_{y1})] \\
\gamma_{s4} &= -\frac{\delta_4}{d_4}[2(w_1 - w_2) + (c_4\psi_{x1} - b_4\psi_{y1}) + (c_4\psi_{x2} - b_4\psi_{y2})]
\end{aligned}\right\} \tag{9-35}$$

where $\gamma_{s1}, \gamma_{s2}, \gamma_{s3}$ and γ_{s4} are the shear strains along sides $\overline{23}$, $\overline{34}$, $\overline{41}$ and $\overline{12}$, respectively; d_1, d_2, d_3 and d_4 are the lengths of sides $\overline{23}$, $\overline{34}$, $\overline{41}$ and $\overline{12}$, respectively (refer to Fig. 9.4).

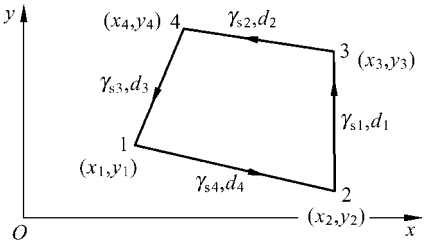

Figure 9.4 The shear strain γ_{si} along each element side and the side length $d_i (i = 1,2,3,4)$

$$\begin{aligned}
&b_1 = y_2 - y_3 \quad b_2 = y_3 - y_4 \quad b_3 = y_4 - y_1 \quad b_4 = y_1 - y_2 \\
&c_1 = x_3 - x_2 \quad c_2 = x_4 - x_3 \quad c_3 = x_1 - x_4 \quad c_4 = x_2 - x_1
\end{aligned} \tag{9-36}$$

$$\delta_i = \frac{6\lambda_i}{1 + 12\lambda_i}, \quad \lambda_i = \frac{D_{di}}{C_{di} d_i^2} \quad (i = 1,2,3,4) \tag{9-37}$$

where D_{di} and C_{di} are given by Eqs. (9-28) and (9-31), respectively. Note that when h approaches zero, δ_i will approach zero. Hence, the transverse shear strains given by Eq. (9-35) will also approach zero.

Let

$$\gamma_{si}^* = d_i \gamma_{si} \quad (i = 1,2,3,4) \tag{9-38}$$

$$\boldsymbol{\gamma}_s^* = [\gamma_{s1}^* \quad \gamma_{s2}^* \quad \gamma_{s3}^* \quad \gamma_{s4}^*]^T \tag{9-39}$$

Then we have

$$\boldsymbol{\gamma}_s^* = \boldsymbol{\Gamma}^* \boldsymbol{q}^e \tag{9-40}$$

where

$$\boldsymbol{\Gamma}^* = [\boldsymbol{\Gamma}_1^* \quad \boldsymbol{\Gamma}_2^* \quad \boldsymbol{\Gamma}_3^* \quad \boldsymbol{\Gamma}_4^*]^{\mathrm{T}}$$

$$\boldsymbol{\Gamma}_1^* = \begin{bmatrix} 0 & 0 & 0 & 0 & 0 \\ 0 & 0 & 0 & 0 & 0 \\ 0 & 0 & 2\delta_3 & -c_3\delta_3 & b_3\delta_3 \\ 0 & 0 & -2\delta_4 & -c_4\delta_4 & b_4\delta_4 \end{bmatrix} \quad \boldsymbol{\Gamma}_2^* = \begin{bmatrix} 0 & 0 & -2\delta_1 & -c_1\delta_1 & b_1\delta_1 \\ 0 & 0 & 0 & 0 & 0 \\ 0 & 0 & 0 & 0 & 0 \\ 0 & 0 & 2\delta_4 & -c_4\delta_4 & b_4\delta_4 \end{bmatrix}$$

$$\boldsymbol{\Gamma}_3^* = \begin{bmatrix} 0 & 0 & 2\delta_1 & -c_1\delta_1 & b_1\delta_1 \\ 0 & 0 & -2\delta_2 & -c_2\delta_2 & b_2\delta_2 \\ 0 & 0 & 0 & 0 & 0 \\ 0 & 0 & 0 & 0 & 0 \end{bmatrix} \quad \boldsymbol{\Gamma}_4^* = \begin{bmatrix} 0 & 0 & 0 & 0 & 0 \\ 0 & 0 & 2\delta_2 & -c_2\delta_2 & b_2\delta_2 \\ 0 & 0 & -2\delta_3 & -c_3\delta_3 & b_3\delta_3 \\ 0 & 0 & 0 & 0 & 0 \end{bmatrix} \tag{9-41}$$

2. Nodal shear strains γ_{xi} and γ_{yi}

The direction cosines of each element side are defined as follows (refer to Fig. 9.5):

$$\left.\begin{aligned} &\cos(s_{12},x) = \cos\theta_1 = \frac{c_4}{d_4},\ \cos(s_{12},y) = \sin\theta_1 = -\frac{b_4}{d_4} \\ &\cos(s_{23},x) = \frac{c_1}{d_1},\ \cos(s_{23},y) = -\frac{b_1}{d_1} \\ &\cos(s_{34},x) = \frac{c_2}{d_2},\ \cos(s_{34},y) = -\frac{b_2}{d_2} \\ &\cos(s_{41},x) = \cos\theta_2 = \frac{c_3}{d_3},\ \cos(s_{41},y) = \sin\theta_2 = -\frac{b_3}{d_3} \end{aligned}\right\} \tag{9-42}$$

With reference to Fig. 9.5, there are two sides, $\overline{41}$ and $\overline{12}$, meeting at the node 1. The shear strain along $\overline{41}$ and $\overline{12}$, γ_{s3} and γ_{s4}, respectively, which are constants, can be expressed in terms of the nodal shear strain (γ_{x1}, γ_{y1}) according to the geometric relation as follows:

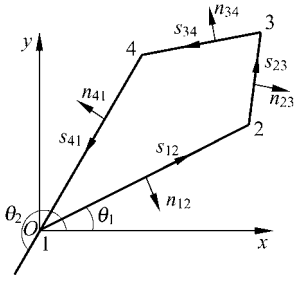

Figure 9.5 The normal and tangential direction along element sides

$$\begin{Bmatrix}\gamma_{s4}\\ \gamma_{s3}\end{Bmatrix}=\begin{bmatrix}\cos(s_{12},x) & \cos(s_{12},y)\\ \cos(s_{41},x) & \cos(s_{41},y)\end{bmatrix}\begin{Bmatrix}\gamma_{x1}\\ \gamma_{y1}\end{Bmatrix}=\begin{bmatrix}\cos\theta_1 & \sin\theta_1\\ \cos\theta_2 & \sin\theta_2\end{bmatrix}\begin{Bmatrix}\gamma_{x1}\\ \gamma_{y1}\end{Bmatrix} \tag{9-43}$$

Note

$$\sin(\theta_2-\theta_1)=\sin\theta_2\cos\theta_1-\cos\theta_2\sin\theta_1=\frac{-b_3c_4+b_4c_3}{d_3d_4} \tag{9-44}$$

therefore, Eqs. (9-43), (9-42) and (9-38) yield

$$\begin{Bmatrix}\gamma_{x1}\\ \gamma_{y1}\end{Bmatrix}=\frac{1}{b_3c_4-b_4c_3}\begin{bmatrix}b_3 & -b_4\\ c_3 & -c_4\end{bmatrix}\begin{Bmatrix}\gamma^*_{s4}\\ \gamma^*_{s3}\end{Bmatrix} \tag{9-45a}$$

Similarly, for node 2 , node 3 and node 4, we obtain

$$\begin{Bmatrix}\gamma_{x2}\\ \gamma_{y2}\end{Bmatrix}=\frac{1}{b_4c_1-b_1c_4}\begin{bmatrix}b_4 & -b_1\\ c_4 & -c_1\end{bmatrix}\begin{Bmatrix}\gamma^*_{s1}\\ \gamma^*_{s4}\end{Bmatrix} \tag{9-45b}$$

$$\begin{Bmatrix}\gamma_{x3}\\ \gamma_{y3}\end{Bmatrix}=\frac{1}{b_1c_2-b_2c_1}\begin{bmatrix}b_1 & -b_2\\ c_1 & -c_2\end{bmatrix}\begin{Bmatrix}\gamma^*_{s2}\\ \gamma^*_{s1}\end{Bmatrix} \tag{9-45c}$$

$$\begin{Bmatrix}\gamma_{x4}\\ \gamma_{y4}\end{Bmatrix}=\frac{1}{b_2c_3-b_3c_2}\begin{bmatrix}b_2 & -b_3\\ c_2 & -c_3\end{bmatrix}\begin{Bmatrix}\gamma^*_{s3}\\ \gamma^*_{s2}\end{Bmatrix} \tag{9-45d}$$

Then we have

$$\left.\begin{aligned}\boldsymbol{\gamma}_{xi}&=\boldsymbol{X}_s\boldsymbol{\gamma}^*_s\\ \boldsymbol{\gamma}_{yi}&=\boldsymbol{Y}_s\boldsymbol{\gamma}^*_s\end{aligned}\right\} \tag{9-46}$$

where

$$\boldsymbol{\gamma}_{xi}=[\gamma_{x1}\quad\gamma_{x2}\quad\gamma_{x3}\quad\gamma_{x4}]^{\mathrm{T}},\quad \boldsymbol{\gamma}_{yi}=[\gamma_{y1}\quad\gamma_{y2}\quad\gamma_{y3}\quad\gamma_{y4}]^{\mathrm{T}} \tag{9-47}$$

$$\boldsymbol{X}_s=\begin{bmatrix}0 & 0 & -\dfrac{b_4}{b_3c_4-b_4c_3} & \dfrac{b_3}{b_3c_4-b_4c_3}\\ \dfrac{b_4}{b_4c_1-b_1c_4} & 0 & 0 & -\dfrac{b_1}{b_4c_1-b_1c_4}\\ -\dfrac{b_2}{b_1c_2-b_2c_1} & \dfrac{b_1}{b_1c_2-b_2c_1} & 0 & 0\\ 0 & -\dfrac{b_3}{b_2c_3-b_3c_2} & \dfrac{b_2}{b_2c_3-b_3c_2} & 0\end{bmatrix} \tag{9-48a}$$

$$\boldsymbol{Y}_{\mathrm{s}}=\begin{bmatrix} 0 & 0 & -\dfrac{c_4}{b_3c_4-b_4c_3} & \dfrac{c_3}{b_3c_4-b_4c_3} \\ \dfrac{c_4}{b_4c_1-b_1c_4} & 0 & 0 & -\dfrac{c_1}{b_4c_1-b_1c_4} \\ -\dfrac{c_2}{b_1c_2-b_2c_1} & \dfrac{c_1}{b_1c_2-b_2c_1} & 0 & 0 \\ 0 & -\dfrac{c_3}{b_2c_3-b_3c_2} & \dfrac{c_2}{b_2c_3-b_3c_2} & 0 \end{bmatrix} \tag{9-48b}$$

3. Interpolation formula for the shear strain fields within the element

The element shear strain fields are assumed as:

$$\left.\begin{aligned} \gamma_x &= \gamma_{x1}N_1^0+\gamma_{x2}N_2^0+\gamma_{x3}N_3^0+\gamma_{x4}N_4^0 \\ \gamma_y &= \gamma_{y1}N_1^0+\gamma_{y2}N_2^0+\gamma_{y3}N_3^0+\gamma_{y4}N_4^0 \end{aligned}\right\} \tag{9-49}$$

where N_i^0 is the bilinear shape function, i.e.,

$$\left.\begin{aligned} N_1^0 &= \frac{1}{4}(1-\xi)(1-\eta) \\ N_2^0 &= \frac{1}{4}(1+\xi)(1-\eta) \\ N_3^0 &= \frac{1}{4}(1+\xi)(1+\eta) \\ N_4^0 &= \frac{1}{4}(1-\xi)(1+\eta) \end{aligned}\right\} \tag{9-50}$$

Substitution of Eqs. (9-40) and (9-46) into Eq. (9-49) yields

$$\boldsymbol{\gamma}=\begin{Bmatrix}\gamma_x\\ \gamma_y\end{Bmatrix}=\begin{bmatrix}\boldsymbol{N}_{\mathrm{s}}^0\boldsymbol{X}_{\mathrm{s}}\boldsymbol{\Gamma}^* \\ \boldsymbol{N}_{\mathrm{s}}^0\boldsymbol{Y}_{\mathrm{s}}\boldsymbol{\Gamma}^*\end{bmatrix}\boldsymbol{q}^e=\boldsymbol{B}_{\mathrm{s}}\boldsymbol{q}^e \tag{9-51}$$

where $\boldsymbol{B}_{\mathrm{s}}$ is the shear strain matrix of the element,

$$\boldsymbol{B}_{\mathrm{s}}=\begin{bmatrix}\boldsymbol{N}_{\mathrm{s}}^0\boldsymbol{X}_{\mathrm{s}}\boldsymbol{\Gamma}^* \\ \boldsymbol{N}_{\mathrm{s}}^0\boldsymbol{Y}_{\mathrm{s}}\boldsymbol{\Gamma}^*\end{bmatrix} \tag{9-52}$$

$$\boldsymbol{N}_{\mathrm{s}}^0=[N_1^0 \quad N_2^0 \quad N_3^0 \quad N_4^0] \tag{9-53}$$

9.3.2 Interpolation Formulas for the Rotation Fields

1. The mid-side normal and tangential rotations of each element side

Let node 5, 6, 7 and 8 be the mid-side nodes of the sides $\overline{23}$, $\overline{34}$, $\overline{41}$ and $\overline{12}$, respectively (refer to Fig. 9.6).

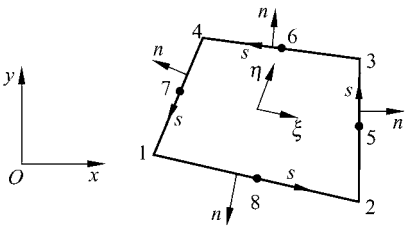

Figure 9.6 The mid-side node of each element side

The normal rotation ψ_n and the tangential rotation ψ_s along side $\overline{23}$ can be expressed as

$$\begin{Bmatrix}\psi_n\\ \psi_s\end{Bmatrix}_{\overline{23}} = \frac{1}{d_1}\begin{bmatrix}-b_1 & -c_1\\ c_1 & -b_1\end{bmatrix}\begin{Bmatrix}\psi_x\\ \psi_y\end{Bmatrix}_{\overline{23}} \tag{9-54}$$

Then, for the node 2 and 3 of the side $\overline{23}$, we obtain

$$\begin{Bmatrix}\psi_{n2}\\ \psi_{s2}\end{Bmatrix}_{\overline{23}} = \frac{1}{d_1}\begin{bmatrix}-b_1 & -c_1\\ c_1 & -b_1\end{bmatrix}\begin{Bmatrix}\psi_{x2}\\ \psi_{y2}\end{Bmatrix}, \quad \begin{Bmatrix}\psi_{n3}\\ \psi_{s3}\end{Bmatrix}_{\overline{23}} = \frac{1}{d_1}\begin{bmatrix}-b_1 & -c_1\\ c_1 & -b_1\end{bmatrix}\begin{Bmatrix}\psi_{x3}\\ \psi_{y3}\end{Bmatrix} \tag{9-55}$$

The variation of the normal rotation ψ_n along each side is assumed to be linear. Therefore, for node 5, we obtain

$$\psi_{n5} = \frac{1}{2}[(\psi_{n2})_{\overline{23}} + (\psi_{n3})_{\overline{23}}] = -\frac{1}{2d_1}[b_1(\psi_{x2}+\psi_{x3}) + c_1(\psi_{y2}+\psi_{y3})] \tag{9-56a}$$

Similarly, for node 6, 7 and 8, we obtain

$$\psi_{n6} = -\frac{1}{2d_2}[b_2(\psi_{x3}+\psi_{x4}) + c_2(\psi_{y3}+\psi_{y4})] \tag{9-56b}$$

$$\psi_{n7} = -\frac{1}{2d_3}[b_3(\psi_{x4}+\psi_{x1}) + c_3(\psi_{y4}+\psi_{y1})] \tag{9-56c}$$

$$\psi_{n8} = -\frac{1}{2d_4}[b_4(\psi_{x1}+\psi_{x2}) + c_4(\psi_{y1}+\psi_{y2})] \tag{9-56d}$$

The tangential rotation ψ_s on the nodes 5,6,7 and 8 can be determined by Eq. (8-99b):

$$\left.\begin{aligned}
\psi_{s5} &= \frac{3}{2d_1}(1-2\delta_1)(w_3-w_2)-\frac{1}{4d_1}(1-6\delta_1)[c_1(\psi_{x2}+\psi_{x3})-b_1(\psi_{y2}+\psi_{y3})]\\
\psi_{s6} &= \frac{3}{2d_2}(1-2\delta_2)(w_4-w_3)-\frac{1}{4d_2}(1-6\delta_2)[c_2(\psi_{x3}+\psi_{x4})-b_2(\psi_{y3}+\psi_{y4})]\\
\psi_{s7} &= \frac{3}{2d_3}(1-2\delta_3)(w_1-w_4)-\frac{1}{4d_3}(1-6\delta_3)[c_3(\psi_{x4}+\psi_{x1})-b_3(\psi_{y4}+\psi_{y1})]\\
\psi_{s8} &= \frac{3}{2d_4}(1-2\delta_4)(w_2-w_1)-\frac{1}{4d_4}(1-6\delta_4)[c_4(\psi_{x1}+\psi_{x2})-b_4(\psi_{y1}+\psi_{y2})]
\end{aligned}\right\} \tag{9-57}$$

2. The rotations ψ_x and ψ_y of the mid-side nodes

For node 5, which is the mid-side node of side $\overline{23}$, (ψ_{5x}, ψ_{5y}) can be obtained from Eq. (9-54) as follows:

$$\begin{Bmatrix}\psi_{x5}\\ \psi_{y5}\end{Bmatrix}=\frac{1}{d_1}\begin{bmatrix}-b_1 & c_1\\ -c_1 & -b_1\end{bmatrix}\begin{Bmatrix}\psi_{n5}\\ \psi_{s5}\end{Bmatrix} \tag{9-58}$$

Similarly, (ψ_{6x}, ψ_{6y}), (ψ_{7x}, ψ_{7y}) and (ψ_{8x}, ψ_{8y}) can be obtained. By coupling these expressions with Eqs. (9-56) and (9-57), we obtain

$$\left.\begin{aligned}\tilde{\boldsymbol{\psi}}_x &= \boldsymbol{F}_x\boldsymbol{q}^e\\ \tilde{\boldsymbol{\psi}}_y &= \boldsymbol{F}_y\boldsymbol{q}^e\end{aligned}\right\} \tag{9-59}$$

where

$$\left.\begin{aligned}\tilde{\boldsymbol{\psi}}_x &= [\psi_{x5}\quad \psi_{x6}\quad \psi_{x7}\quad \psi_{x8}]^{\mathrm{T}}\\ \tilde{\boldsymbol{\psi}}_y &= [\psi_{y5}\quad \psi_{y6}\quad \psi_{y7}\quad \psi_{y8}]^{\mathrm{T}}\end{aligned}\right\} \tag{9-60}$$

$$\boldsymbol{F}_x = [\,\boldsymbol{F}_{x1}\quad \boldsymbol{F}_{x2}\quad \boldsymbol{F}_{x3}\quad \boldsymbol{F}_{x4}\,] \tag{9-61}$$

$$\boldsymbol{F}_y = [\,\boldsymbol{F}_{y1}\quad \boldsymbol{F}_{y2}\quad \boldsymbol{F}_{y3}\quad \boldsymbol{F}_{y4}\,] \tag{9-62}$$

$$\boldsymbol{F}_{x1}=\begin{bmatrix}
0 & 0 & 0 & 0 & 0\\
0 & 0 & 0 & 0 & 0\\
0 & 0 & \frac{3c_3}{2d_3^2}(1-2\delta_3) & \frac{1}{2d_3^2}\left[b_3^2-\frac{c_3^2}{2}(1-6\delta_3)\right] & \frac{3b_3c_3}{4d_3^2}(1-2\delta_3)\\
0 & 0 & -\frac{3c_4}{2d_4^2}(1-2\delta_4) & \frac{1}{2d_4^2}\left[b_4^2-\frac{c_4^2}{2}(1-6\delta_4)\right] & \frac{3b_4c_4}{4d_4^2}(1-2\delta_4)
\end{bmatrix} \tag{9-63a}$$

$$\boldsymbol{F}_{x2}=\begin{bmatrix} 0 & 0 & -\dfrac{3c_1}{2d_1^2}(1-2\delta_1) & \dfrac{1}{2d_1^2}\left[b_1^2-\dfrac{c_1^2}{2}(1-6\delta_1)\right] & \dfrac{3b_1c_1}{4d_1^2}(1-2\delta_1) \\ 0 & 0 & 0 & 0 & 0 \\ 0 & 0 & 0 & 0 & 0 \\ 0 & 0 & \dfrac{3c_4}{2d_4^2}(1-2\delta_4) & \dfrac{1}{2d_4^2}\left[b_4^2-\dfrac{c_4^2}{2}(1-6\delta_4)\right] & \dfrac{3b_4c_4}{4d_4^2}(1-2\delta_4) \end{bmatrix} \tag{9-63b}$$

$$\boldsymbol{F}_{x3}=\begin{bmatrix} 0 & 0 & \dfrac{3c_1}{2d_1^2}(1-2\delta_1) & \dfrac{1}{2d_1^2}\left[b_1^2-\dfrac{c_1^2}{2}(1-6\delta_1)\right] & \dfrac{3b_1c_1}{4d_1^2}(1-2\delta_1) \\ 0 & 0 & -\dfrac{3c_2}{2d_2^2}(1-2\delta_2) & \dfrac{1}{2d_2^2}\left[b_2^2-\dfrac{c_2^2}{2}(1-6\delta_2)\right] & \dfrac{3b_2c_2}{4d_2^2}(1-2\delta_2) \\ 0 & 0 & 0 & 0 & 0 \\ 0 & 0 & 0 & 0 & 0 \end{bmatrix} \tag{9-63c}$$

$$\boldsymbol{F}_{x4}=\begin{bmatrix} 0 & 0 & 0 & 0 & 0 \\ 0 & 0 & \dfrac{3c_2}{2d_2^2}(1-2\delta_2) & \dfrac{1}{2d_2^2}\left[b_2^2-\dfrac{c_2^2}{2}(1-6\delta_2)\right] & \dfrac{3b_2c_2}{4d_2^2}(1-2\delta_2) \\ 0 & 0 & -\dfrac{3c_3}{2d_3^2}(1-2\delta_3) & \dfrac{1}{2d_3^2}\left[b_3^2-\dfrac{c_3^2}{2}(1-6\delta_3)\right] & \dfrac{3b_3c_3}{4d_3^2}(1-2\delta_3) \\ 0 & 0 & 0 & 0 & 0 \end{bmatrix} \tag{9-63d}$$

$$\boldsymbol{F}_{y1}=\begin{bmatrix} 0 & 0 & 0 & 0 & 0 \\ 0 & 0 & 0 & 0 & 0 \\ 0 & 0 & -\dfrac{3b_3}{2d_3^2}(1-2\delta_3) & \dfrac{3b_3c_3}{4d_3^2}(1-2\delta_3) & \dfrac{1}{2d_3^2}\left[c_3^2-\dfrac{b_3^2}{2}(1-6\delta_3)\right] \\ 0 & 0 & \dfrac{3b_4}{2d_4^2}(1-2\delta_4) & \dfrac{3b_4c_4}{4d_4^2}(1-2\delta_4) & \dfrac{1}{2d_4^2}\left[c_4^2-\dfrac{b_4^2}{2}(1-6\delta_4)\right] \end{bmatrix} \tag{9-64a}$$

$$\boldsymbol{F}_{y2}=\begin{bmatrix} 0 & 0 & \dfrac{3b_1}{2d_1^2}(1-2\delta_1) & \dfrac{3b_1c_1}{4d_1^2}(1-2\delta_1) & \dfrac{1}{2d_1^2}\left[c_1^2-\dfrac{b_1^2}{2}(1-6\delta_1)\right] \\ 0 & 0 & 0 & 0 & 0 \\ 0 & 0 & 0 & 0 & 0 \\ 0 & 0 & -\dfrac{3b_4}{2d_4^2}(1-2\delta_4) & \dfrac{3b_4c_4}{4d_4^2}(1-2\delta_4) & \dfrac{1}{2d_4^2}\left[c_4^2-\dfrac{b_4^2}{2}(1-6\delta_4)\right] \end{bmatrix} \tag{9-64b}$$

$$\boldsymbol{F}_{y3}=\begin{bmatrix} 0 & 0 & -\dfrac{3b_1}{2d_1^2}(1-2\delta_1) & \dfrac{3b_1c_1}{4d_1^2}(1-2\delta_1) & \dfrac{1}{2d_1^2}\left[c_1^2-\dfrac{b_1^2}{2}(1-6\delta_1)\right] \\ 0 & 0 & \dfrac{3b_2}{2d_2^2}(1-2\delta_2) & \dfrac{3b_2c_2}{4d_2^2}(1-2\delta_2) & \dfrac{1}{2d_2^2}\left[c_2^2-\dfrac{b_2^2}{2}(1-6\delta_2)\right] \\ 0 & 0 & 0 & 0 & 0 \\ 0 & 0 & 0 & 0 & 0 \end{bmatrix} \tag{9-64c}$$

$$\boldsymbol{F}_{y4}=\begin{bmatrix} 0 & 0 & 0 & 0 & 0 \\ 0 & 0 & -\dfrac{3b_2}{2d_2^2}(1-2\delta_2) & \dfrac{3b_2c_2}{4d_2^2}(1-2\delta_2) & \dfrac{1}{2d_2^2}\left[c_2^2-\dfrac{b_2^2}{2}(1-6\delta_2)\right] \\ 0 & 0 & \dfrac{3b_3}{2d_3^2}(1-2\delta_3) & \dfrac{3b_3c_3}{4d_3^2}(1-2\delta_3) & \dfrac{1}{2d_3^2}\left[c_3^2-\dfrac{b_3^2}{2}(1-6\delta_3)\right] \\ 0 & 0 & 0 & 0 & 0 \end{bmatrix} \tag{9-64d}$$

3. Interpolation formulas for the rotation fields ψ_x and ψ_y within the element

The rotation fields ψ_x and ψ_y within the element can be expressed in terms of the node rotations ψ_{xi} and ψ_{yi} ($i=1, 2, \cdots, 8$):

$$\left.\begin{aligned} \psi_x &= \sum_{i=1}^{8} N_i \psi_{xi} \\ \psi_y &= \sum_{i=1}^{8} N_i \psi_{yi} \end{aligned}\right\} \tag{9-65}$$

where

$$\left.\begin{aligned} N_1 &= -\frac{1}{4}(1-\xi)(1-\eta)(1+\xi+\eta) & N_5 &= \frac{1}{2}(1-\eta^2)(1+\xi) \\ N_2 &= -\frac{1}{4}(1+\xi)(1-\eta)(1-\xi+\eta) & N_6 &= \frac{1}{2}(1-\xi^2)(1+\eta) \\ N_3 &= -\frac{1}{4}(1+\xi)(1+\eta)(1-\xi-\eta) & N_7 &= \frac{1}{2}(1-\eta^2)(1-\xi) \\ N_4 &= -\frac{1}{4}(1-\xi)(1+\eta)(1+\xi-\eta) & N_8 &= \frac{1}{2}(1-\xi^2)(1-\eta) \end{aligned}\right\} \tag{9-66}$$

Substituting Eq. (9-59) into Eq. (9-65), the element rotation fields ψ_x and ψ_y can be expressed by the element nodal displacement vector $\boldsymbol{q}^e$.

9.3.3 Interpolation Formulas for the In-Plane Displacement Fields of the Mid-Plane

The in-plane displacement fields u^0 and v^0 of the mid-plane can be expressed as:

$$\left.\begin{aligned} u^0 &= \sum_{i=1}^{4} N_i^0 u_i \\ v^0 &= \sum_{i=1}^{4} N_i^0 v_i \end{aligned}\right\} \tag{9-67}$$

where N_i^0 is given by Eq. (9-50).

9.3.4 The In-Plane Strain and Curvature Fields

The in-plane strain (9-4) of the mid-plane can be rewritten as:

$$\boldsymbol{\varepsilon}^0 = \boldsymbol{B}^0 \boldsymbol{q}^e \tag{9-68}$$

where

$$\boldsymbol{B}^0 = [\boldsymbol{B}_1^0 \quad \boldsymbol{B}_2^0 \quad \boldsymbol{B}_3^0 \quad \boldsymbol{B}_4^0] \tag{9-69}$$

$$\boldsymbol{B}_i^0 = \begin{bmatrix} \dfrac{\partial N_i^0}{\partial x} & 0 & 0 & 0 & 0 \\ 0 & \dfrac{\partial N_i^0}{\partial y} & 0 & 0 & 0 \\ \dfrac{\partial N_i^0}{\partial y} & \dfrac{\partial N_i^0}{\partial x} & 0 & 0 & 0 \end{bmatrix} \quad (i = 1,2,3,4) \tag{9-70}$$

$$\begin{Bmatrix} \dfrac{\partial}{\partial x} \\ \dfrac{\partial}{\partial y} \end{Bmatrix} = \boldsymbol{J}^{-1} \begin{Bmatrix} \dfrac{\partial}{\partial \xi} \\ \dfrac{\partial}{\partial \eta} \end{Bmatrix} \tag{9-71}$$

$\boldsymbol{J}^{-1}$ is the Jacobian inverse, and it is the same as that of the bilinear isoparametric quadrilateral element Q4.

From Eqs. (9-5), (9-65) and (9-59), the curvature fields can be rewritten as:

$$\boldsymbol{\kappa} = -(\boldsymbol{H}_0 + \boldsymbol{H}_1 \boldsymbol{F}_x + \boldsymbol{H}_2 \boldsymbol{F}_y)\boldsymbol{q}^e = \boldsymbol{B}_\mathrm{b} \boldsymbol{q}^e \tag{9-72}$$

where $\boldsymbol{B}_{\mathrm{b}}$ is the bending strain matrix:

$$\boldsymbol{B}_{\mathrm{b}} = [\, \boldsymbol{B}_{\mathrm{b1}} \quad \boldsymbol{B}_{\mathrm{b2}} \quad \boldsymbol{B}_{\mathrm{b3}} \quad \boldsymbol{B}_{\mathrm{b4}} \,] \tag{9-73}$$

$$\boldsymbol{H}_0 = [\, \boldsymbol{H}_{01} \quad \boldsymbol{H}_{02} \quad \boldsymbol{H}_{03} \quad \boldsymbol{H}_{04} \,] \tag{9-74}$$

$$\boldsymbol{H}_{0i} = \begin{bmatrix} 0 & 0 & 0 & \dfrac{\partial N_i}{\partial x} & 0 \\ 0 & 0 & 0 & 0 & \dfrac{\partial N_i}{\partial y} \\ 0 & 0 & 0 & \dfrac{\partial N_i}{\partial y} & \dfrac{\partial N_i}{\partial x} \end{bmatrix} \quad (i = 1,2,3,4) \tag{9-75}$$

$$\boldsymbol{H}_1 = \begin{bmatrix} \dfrac{\partial N_5}{\partial x} & \dfrac{\partial N_6}{\partial x} & \dfrac{\partial N_7}{\partial x} & \dfrac{\partial N_8}{\partial x} \\ 0 & 0 & 0 & 0 \\ \dfrac{\partial N_5}{\partial y} & \dfrac{\partial N_6}{\partial y} & \dfrac{\partial N_7}{\partial y} & \dfrac{\partial N_8}{\partial y} \end{bmatrix}, \quad \boldsymbol{H}_2 = \begin{bmatrix} 0 & 0 & 0 & 0 \\ \dfrac{\partial N_5}{\partial y} & \dfrac{\partial N_6}{\partial y} & \dfrac{\partial N_7}{\partial y} & \dfrac{\partial N_8}{\partial y} \\ \dfrac{\partial N_5}{\partial x} & \dfrac{\partial N_6}{\partial x} & \dfrac{\partial N_7}{\partial x} & \dfrac{\partial N_8}{\partial x} \end{bmatrix} \tag{9-76a,b}$$

where $N_i (i = 1,2,\cdots,8)$ is given by Eq. (9-66).

Then, the $\boldsymbol{\varepsilon}_{\mathrm{p}}$ in Eq. (9-14) can be expressed as:

$$\boldsymbol{\varepsilon}_{\mathrm{p}} = \begin{Bmatrix} \boldsymbol{\varepsilon}^0 \\ \boldsymbol{\kappa} \end{Bmatrix} = \begin{bmatrix} \boldsymbol{B}^0 \\ \boldsymbol{B}_{\mathrm{b}} \end{bmatrix} \boldsymbol{q}^e = \boldsymbol{B}_{\mathrm{p}} \boldsymbol{q}^e \tag{9-77}$$

9.3.5 The Stiffness Matrix of the Element

The element strain energy is:

$$U^e = \frac{1}{2} \boldsymbol{q}^{e\mathrm{T}} \iint_{A^e} \boldsymbol{B}_{\mathrm{p}}{}^{\mathrm{T}} \boldsymbol{C}_{\mathrm{p}} \boldsymbol{B}_{\mathrm{p}} \mathrm{d}A \, \boldsymbol{q}^e + \frac{1}{2} \boldsymbol{q}^{e\mathrm{T}} \iint_{A^e} \boldsymbol{B}_{\mathrm{s}}{}^{\mathrm{T}} \boldsymbol{C}_{\mathrm{s}} \boldsymbol{B}_{\mathrm{s}} \mathrm{d}A \, \boldsymbol{q}^e \tag{9-78}$$

where A^e is the area of the element; $\boldsymbol{C}_{\mathrm{p}}$ and $\boldsymbol{C}_{\mathrm{s}}$ are given by Eqs. (9-14) and (9-19), respectively. The element stiffness matrix is

$$\begin{aligned} \boldsymbol{K}^e &= \iint_{A^e} \boldsymbol{B}_{\mathrm{p}}{}^{\mathrm{T}} \boldsymbol{C}_{\mathrm{p}} \boldsymbol{B}_{\mathrm{p}} \mathrm{d}A + \iint_{A^e} \boldsymbol{B}_{\mathrm{s}}{}^{\mathrm{T}} \boldsymbol{C}_{\mathrm{s}} \boldsymbol{B}_{\mathrm{s}} \mathrm{d}A \\ &= \int_{-1}^{1} \int_{-1}^{1} \boldsymbol{B}_{\mathrm{p}}{}^{\mathrm{T}} \boldsymbol{C}_{\mathrm{p}} \boldsymbol{B}_{\mathrm{p}} \left| \boldsymbol{J} \right| \mathrm{d}\xi \mathrm{d}\eta + \int_{-1}^{1} \int_{-1}^{1} \boldsymbol{B}_{\mathrm{s}}{}^{\mathrm{T}} \boldsymbol{C}_{\mathrm{s}} \boldsymbol{B}_{\mathrm{s}} \left| \boldsymbol{J} \right| \mathrm{d}\xi \mathrm{d}\eta \end{aligned} \tag{9-79}$$

where $|\boldsymbol{J}|$ is the Jacobian determinant.

A standard 2×2 Gauss integration scheme is found to be sufficient for the calculation of Eq. (9-79), even though 3×3 integration is theoretically necessary. No spurious mode is presented in the element. Note that this 2×2 scheme should not be confused with the standard reduced integration scheme because both 2×2 and 3×3 integration schemes can avoid the shear locking problem and give proper solutions.

This element is denoted as CTMQ20.

9.3.6 Element Load Vector

The deflection field w is not used during the course of calculating the element stiffness matrix. But, for calculating the effective load vector, w can be assumed as follows:

$$w = \boldsymbol{N}_w \boldsymbol{q}^e \tag{9-80}$$

with

$$\boldsymbol{N}_w = [0 \quad 0 \quad N_1^0 \quad 0 \quad 0 \,\vdots\, 0 \quad 0 \quad N_2^0 \quad 0 \quad 0 \,\vdots\, 0 \quad 0 \quad N_3^0 \quad 0 \quad 0 \,\vdots\, 0 \quad 0 \quad N_4^0 \quad 0 \quad 0] \tag{9-81}$$

where N_i^0 is given in Eq. (9-50). Then, the element equivalent nodal forces due to a pressure $\overline{q}(x,y)$ can be given by

$$\boldsymbol{f}^e = [0 \quad 0 \quad f_{z1} \quad 0 \quad 0 \,\vdots\, 0 \quad 0 \quad f_{z2} \quad 0 \quad 0 \,\vdots\, 0 \quad 0 \quad f_{z3} \quad 0 \quad 0 \,\vdots\, 0 \quad 0 \quad f_{z4} \quad 0 \quad 0]^{\mathrm{T}} \tag{9-82}$$

with $$f_{zi} = \int_{A^e} \overline{q}(x,y) N_i^0 \mathrm{d}A = \int_{-1}^{1}\int_{-1}^{1} \overline{q}^*(\xi,\eta) N_i^0 |\boldsymbol{J}| \mathrm{d}\xi \mathrm{d}\eta \quad (i = 1,2,3,4) \tag{9-83}$$

9.4 The Hybrid-Enhanced Post-Processing Procedure for Element Stresses

According to the standard procedure of displacement-based elements, the stress solutions of the plate element can be solved from the stress-strain relations (9-10) and (9-11). But, the transverse shear stress solutions obtained from Eq. (9-11) are all constants at each layer of the plate, which neither reflect the actual nonlinear continuous distributions of the transverse shear stresses, nor satisfy the zero shear stress conditions on the bounding planes of the plate. When the 3D elasticity differential equilibrium equations are used to compute the transverse shear stresses, the procedure for the displacement-based elements is quite complicated, and hard

to obtain satisfactory results. Reference [26] proposed a simple hybrid-enhanced post-processing procedure to improve the internal force solutions of the displacement-based plate elements, and references [22,23] employed this procedure to evaluate the internal forces and stresses of the laminated composite plate elements. More accurate results for stresses, especially for the transverse shear stresses, can be obtained. So the element CTMQ20, which uses this treatment, possesses the advantages of both the displacement-based and hybrid elements.

9.4.1 The Bending Moment and Shear Force Fields

The bending moment field $\boldsymbol{M}$ can be assumed as follows[26,27]:

$$\boldsymbol{M} = \boldsymbol{P}_M \boldsymbol{\lambda}_M \tag{9-84}$$

in which

$$\boldsymbol{M} = [M_x \quad M_y \quad M_{xy}]^{\mathrm{T}} \tag{9-85}$$

$$\boldsymbol{P}_M = \begin{bmatrix} 1 & \xi & \eta & \xi\eta & 0 & 0 & 0 & 0 & 0 & 0 & 0 & 0 \\ 0 & 0 & 0 & 0 & 1 & \xi & \eta & \xi\eta & 0 & 0 & 0 & 0 \\ 0 & 0 & 0 & 0 & 0 & 0 & 0 & 0 & 1 & \xi & \eta & \xi\eta \end{bmatrix} \tag{9-86}$$

$$\boldsymbol{\lambda}_M = [\lambda_1 \quad \lambda_2 \quad \lambda_3 \quad \lambda_4 \quad \lambda_5 \quad \lambda_6 \quad \lambda_7 \quad \lambda_8 \quad \lambda_9 \quad \lambda_{10} \quad \lambda_{11} \quad \lambda_{12}]^{\mathrm{T}} \tag{9-87}$$

where (ξ, η) are the isoparametric coordinates of the quadrilateral element; λ_i $(i = 1, 2, \cdots, 12)$ are 12 unknown parameters.

And, the shear field is assumed to satisfy the homogeneous equilibrium equation,

$$\boldsymbol{Q} = \begin{Bmatrix} Q_x \\ Q_y \end{Bmatrix} = \begin{Bmatrix} M_{x,x} + M_{xy,y} \\ M_{xy,x} + M_{y,y} \end{Bmatrix} = \boldsymbol{P}_Q \boldsymbol{\lambda}_M \tag{9-88}$$

in which

$$\boldsymbol{P}_Q = \begin{bmatrix} 0 & j_{11} & j_{12} & j_{11}\eta + j_{12}\xi & 0 & 0 & 0 & 0 & 0 & j_{21} & j_{22} & j_{21}\eta + j_{22}\xi \\ 0 & 0 & 0 & 0 & 0 & j_{21} & j_{22} & j_{21}\eta + j_{22}\xi & 0 & j_{11} & j_{12} & j_{11}\eta + j_{12}\xi \end{bmatrix} \tag{9-89}$$

j_{11}, j_{12}, j_{21} and j_{22} are the components of the Jacobian inverse.

9.4.2 The Membrane Force Field of the Mid-Plane

The membrane force field $\boldsymbol{N}$ can be assumed as follows[28]:

$$\boldsymbol{N} = \boldsymbol{P}_N \boldsymbol{\lambda}_N \tag{9-90}$$

in which

$$\boldsymbol{P}_N = \begin{bmatrix} 1 & 0 & 0 & \overline{a}_1^2\eta & \overline{a}_3^2\xi \\ 0 & 1 & 0 & \overline{b}_1^2\eta & \overline{b}_3^2\xi \\ 0 & 0 & 1 & \overline{a}_1\overline{b}_1\eta & \overline{a}_3\overline{b}_3\xi \end{bmatrix} \tag{9-91}$$

$$\left.\begin{aligned} \overline{a}_1 &= \frac{1}{4}(-x_1 + x_2 + x_3 - x_4) \quad \overline{b}_1 = \frac{1}{4}(-y_1 + y_2 + y_3 - y_4) \\ \overline{a}_3 &= \frac{1}{4}(-x_1 - x_2 + x_3 + x_4) \quad \overline{b}_3 = \frac{1}{4}(-y_1 - y_2 + y_3 + y_4) \end{aligned}\right\} \tag{9-92}$$

$$\boldsymbol{\lambda}_N = [\lambda_{13} \quad \lambda_{14} \quad \lambda_{15} \quad \lambda_{16} \quad \lambda_{17}]^{\mathrm{T}} \tag{9-93}$$

λ_i ($i = 13, 14, \cdots, 17$) are 5 unknown parameters.

9.4.3 The Condensation Procedure

Equations (9-14) and (9-15) can be rewritten as:

$$\boldsymbol{\sigma}_{\mathrm{p}} = \begin{Bmatrix} \boldsymbol{N} \\ \boldsymbol{M} \end{Bmatrix} = \begin{bmatrix} \boldsymbol{P}_N & \boldsymbol{0}_{3\times 12} \\ \boldsymbol{0}_{3\times 5} & \boldsymbol{P}_M \end{bmatrix} \begin{Bmatrix} \boldsymbol{\lambda}_N \\ \boldsymbol{\lambda}_M \end{Bmatrix} = \boldsymbol{P}_{NM} \boldsymbol{\lambda}_{NM} \tag{9-94}$$

$$\boldsymbol{Q} = \begin{bmatrix} \boldsymbol{0}_{2\times 5} & \boldsymbol{P}_Q \end{bmatrix} \begin{Bmatrix} \boldsymbol{\lambda}_N \\ \boldsymbol{\lambda}_M \end{Bmatrix} = \boldsymbol{P}_{NQ} \boldsymbol{\lambda}_{NM} \tag{9-95}$$

By employing the Hellinger-Reissner variational principle, the energy functional of the laminated composite plate element can be expressed as:

$$\begin{aligned} \Pi_R^e &= -\frac{1}{2}\iint_{A^e} \boldsymbol{\sigma}_{\mathrm{p}}{}^{\mathrm{T}} \boldsymbol{S}_{\mathrm{p}} \boldsymbol{\sigma}_{\mathrm{p}} \mathrm{d}A - \frac{1}{2}\iint_{A^e} \boldsymbol{Q}^{\mathrm{T}} \boldsymbol{S}_{\mathrm{s}} \boldsymbol{Q} \mathrm{d}A + \iint_{A^e} \boldsymbol{\sigma}_{\mathrm{p}}{}^{\mathrm{T}} \boldsymbol{\varepsilon}_{\mathrm{p}} \mathrm{d}A + \iint_{A^e} \boldsymbol{Q}^{\mathrm{T}} \boldsymbol{\gamma} \mathrm{d}A - W_{\exp} \\ &= -\frac{1}{2} \boldsymbol{\lambda}_{NM}{}^{\mathrm{T}} \iint_{A^e} (\boldsymbol{P}_{NM}{}^{\mathrm{T}} \boldsymbol{S}_{\mathrm{p}} \boldsymbol{P}_{NM} + \boldsymbol{P}_{NQ}{}^{\mathrm{T}} \boldsymbol{S}_{\mathrm{s}} \boldsymbol{P}_{NQ}) \mathrm{d}A \cdot \boldsymbol{\lambda}_{NM} \\ &\quad + \boldsymbol{\lambda}_{NM}{}^{\mathrm{T}} \iint_{A^e} (\boldsymbol{P}_{NM}{}^{\mathrm{T}} \boldsymbol{B}_{\mathrm{p}} + \boldsymbol{P}_{NQ}{}^{\mathrm{T}} \boldsymbol{B}_{\mathrm{s}}) \mathrm{d}A \cdot \boldsymbol{q}^e - W_{\exp} \end{aligned} \tag{9-96}$$

where $W_{\exp}$ is the work done by external forces.

From the stationary condition $\dfrac{\partial \Pi_R^e}{\partial \boldsymbol{\lambda}_{NM}} = \boldsymbol{0}$, we obtain:

$$\boldsymbol{\lambda}_{NM} = -\boldsymbol{K}_{\lambda\lambda}^{-1}\boldsymbol{K}_{\lambda q}\boldsymbol{q}^{e} \tag{9-97}$$

where

$$\begin{aligned}\boldsymbol{K}_{\lambda\lambda} &= -\iint_{A^e}(\boldsymbol{P}_{NM}^{\mathrm{T}}\boldsymbol{S}_{\mathrm{p}}\boldsymbol{P}_{NM} + \boldsymbol{P}_{NQ}^{\mathrm{T}}\boldsymbol{S}_{\mathrm{s}}\boldsymbol{P}_{NQ})\mathrm{d}A \\ \boldsymbol{K}_{\lambda q} &= \iint_{A^e}(\boldsymbol{P}_{NM}^{\mathrm{T}}\boldsymbol{B}_{\mathrm{p}} + \boldsymbol{P}_{NQ}^{\mathrm{T}}\boldsymbol{B}_{\mathrm{s}})\mathrm{d}A\end{aligned} \tag{9-98}$$

Substituting Eq. (9-97) into Eqs. (9-94) and (9-95), $\boldsymbol{N}$, $\boldsymbol{M}$ and $\boldsymbol{Q}$ can be obtained. And, the element stresses of each layer can be obtained by Eq. (9-27).

9.4.4 Recovery of the Transverse Shear Stresses

Ignoring the effects of the body forces, the stresses of the laminated composite plate should satisfy the following homogeneous equations:

$$\left.\begin{aligned}\frac{\partial\sigma_x}{\partial x} + \frac{\partial\tau_{xy}}{\partial y} + \frac{\partial\tau_{xz}}{\partial z} = 0 \\ \frac{\partial\tau_{xy}}{\partial x} + \frac{\partial\sigma_y}{\partial y} + \frac{\partial\tau_{yz}}{\partial z} = 0\end{aligned}\right\} \tag{9-99}$$

For the kth layer of the plate, we obtain

$$\begin{aligned}\boldsymbol{\tau}_{zk} &= -\int_{-h/2}^{z}\boldsymbol{\partial}\boldsymbol{\sigma}_k\mathrm{d}z = -\int_{-h/2}^{z}\boldsymbol{\partial}\bar{\boldsymbol{Q}}_k(\boldsymbol{S}_e + z\boldsymbol{S}_{\mathrm{b}})\boldsymbol{\sigma}_{\mathrm{p}}\mathrm{d}z \\ &= -\int_{-h/2}^{z}[\overline{\boldsymbol{Bl}}_1\bar{\boldsymbol{Q}}_k(\boldsymbol{S}_e + z\boldsymbol{S}_{\mathrm{b}})\boldsymbol{\sigma}_{\mathrm{p},x} + \overline{\boldsymbol{Bl}}_2\bar{\boldsymbol{Q}}_k(\boldsymbol{S}_e + z\boldsymbol{S}_{\mathrm{b}})\boldsymbol{\sigma}_{\mathrm{p},y}]\mathrm{d}z\end{aligned} \tag{9-100}$$

in which

$$\boldsymbol{\partial} = \begin{bmatrix}\dfrac{\partial}{\partial x} & 0 & \dfrac{\partial}{\partial y} \\ 0 & \dfrac{\partial}{\partial y} & \dfrac{\partial}{\partial x}\end{bmatrix} \tag{9-101}$$

$$\overline{\boldsymbol{Bl}}_1 = \begin{bmatrix}1 & 0 & 0 \\ 0 & 0 & 1\end{bmatrix}, \quad \overline{\boldsymbol{Bl}}_2 = \begin{bmatrix}0 & 0 & 1 \\ 0 & 1 & 0\end{bmatrix} \tag{9-102a,b}$$

$$\begin{aligned}\boldsymbol{\sigma}_{\mathrm{p},x} &= -\boldsymbol{P}_{NM,x}\boldsymbol{K}_{\lambda\lambda}^{-1}\boldsymbol{K}_{\lambda q}\boldsymbol{q}^{e} \\ \boldsymbol{\sigma}_{\mathrm{p},y} &= -\boldsymbol{P}_{NM,y}\boldsymbol{K}_{\lambda\lambda}^{-1}\boldsymbol{K}_{\lambda q}\boldsymbol{q}^{e}\end{aligned} \tag{9-103}$$

(, x) and (, y) denote the derivatives with respect to x and y of all components in a matrix.

Finally, we obtain

$$\begin{aligned}\boldsymbol{\tau}_{zk} = &-\overline{\boldsymbol{Bl}}_1\bar{\boldsymbol{Q}}_k[(z-h_{k-1})\boldsymbol{S}_e+\frac{1}{2}(z^2-h_{k-1}^2)\boldsymbol{S}_{\mathrm{b}}]\boldsymbol{\sigma}_{\mathrm{p},x}\\ &-\overline{\boldsymbol{Bl}}_2\bar{\boldsymbol{Q}}_k[(z-h_{k-1})\boldsymbol{S}_e+\frac{1}{2}(z^2-h_{k-1}^2)\boldsymbol{S}_{\mathrm{b}}]\boldsymbol{\sigma}_{\mathrm{p},y}\\ &-\sum_{i=1}^{k-1}\overline{\boldsymbol{Bl}}_1\bar{\boldsymbol{Q}}_k[(h_i-h_{i-1})\boldsymbol{S}_e+\frac{1}{2}(h_i^2-h_{i-1}^2)\boldsymbol{S}_{\mathrm{b}}]\boldsymbol{\sigma}_{\mathrm{p},x}\\ &-\sum_{i=1}^{k-1}\overline{\boldsymbol{Bl}}_2\bar{\boldsymbol{Q}}_k[(h_i-h_{i-1})\boldsymbol{S}_e+\frac{1}{2}(h_i^2-h_{i-1}^2)\boldsymbol{S}_{\mathrm{b}}]\boldsymbol{\sigma}_{\mathrm{p},y}\end{aligned} \tag{9-104}$$

9.5 Vibration Analysis of Laminated Composite Plates

The in-plane displacement field of the element CTMQ20 can be obtained from Eq. (9-67):

$$\begin{Bmatrix}u^0\\ v^0\end{Bmatrix} = \boldsymbol{N}^0\boldsymbol{q}^e \tag{9-105}$$

where

$$\boldsymbol{N}^0 = [\boldsymbol{N}_1^0 \quad \boldsymbol{N}_2^0 \quad \boldsymbol{N}_3^0 \quad \boldsymbol{N}_4^0] \tag{9-106}$$

$$\boldsymbol{N}_i^0 = \begin{bmatrix}N_i^0 & 0 & 0 & 0 & 0\\ 0 & N_i^0 & 0 & 0 & 0\end{bmatrix} \quad (i=1,2,3,4) \tag{9-107}$$

The rotation field of the element CTMQ20 can be obtained from Eqs. (9-59) and (9-65):

$$\begin{Bmatrix}\psi_x\\ \psi_y\end{Bmatrix} = \boldsymbol{N}_\beta\boldsymbol{q}^e \tag{9-108}$$

where

$$\boldsymbol{N}_\beta = \boldsymbol{N}_{\beta 1} + \boldsymbol{N}_{\beta 2} \tag{9-109}$$

$$\boldsymbol{N}_{\beta 1} = \begin{bmatrix}0&0&0&N_1&0&0&0&0&N_2&0&0&0&0&N_3&0&0&0&0&N_4&0\\ 0&0&0&0&N_1&0&0&0&0&N_2&0&0&0&0&N_3&0&0&0&0&N_4\end{bmatrix} \tag{9-110}$$

$$\boldsymbol{N}_{\beta 2}=\begin{bmatrix}\tilde{\boldsymbol{N}}_{\beta}\boldsymbol{F}_{x}\\ \tilde{\boldsymbol{N}}_{\beta}\boldsymbol{F}_{y}\end{bmatrix} \tag{9-111}$$

$$\tilde{\boldsymbol{N}}_{\beta}=\begin{bmatrix}N_5 & N_6 & N_7 & N_8\end{bmatrix} \tag{9-112}$$

For the deflection field w, the expression (9-80) is not the real deflection field of the element CTMQ20, which must be derived from the relation (9-6). In order to avoid complicated derivation, the following element concentrated mass matrix corresponding to the deflection field w is suggested here:

$$\boldsymbol{m}_{w}^{e}=\frac{\rho Ah}{4}\begin{bmatrix}\boldsymbol{a} & & & \\ & \boldsymbol{a} & & \\ & & \boldsymbol{a} & \\ & & & \boldsymbol{a}\end{bmatrix} \tag{9-113}$$

where ρ is mass density of the plate; A is the area of the element, and

$$\boldsymbol{a}=\begin{bmatrix}0 & & & & \\ & 0 & & & \\ & & 1 & & \\ & & & 0 & \\ & & & & 0\end{bmatrix}$$

Then the expression of the element mass matrix $\boldsymbol{m}^{e}$ can be written as:

$$\boldsymbol{m}^{e}=\boldsymbol{m}_{w}^{e}+\boldsymbol{m}_{0}^{e}+\boldsymbol{m}_{\beta}^{e} \tag{9-114}$$

where $\boldsymbol{m}_{0}{}^{e}$ is the in-plane mass matrix:

$$\boldsymbol{m}_{0}{}^{e}=\rho h\int_{-1}^{1}\int_{-1}^{1}(\boldsymbol{N}^{0})^{\mathrm{T}}\boldsymbol{N}^{0}\left|\boldsymbol{J}\right|\mathrm{d}\xi\mathrm{d}\eta \tag{9-115}$$

$\boldsymbol{m}_{\beta}^{e}$ is the mass matrix caused by the moment of inertia:

$$\boldsymbol{m}_{\beta}{}^{e}=\frac{\rho h^{3}}{12}\int_{-1}^{1}\int_{-1}^{1}\boldsymbol{N}_{\beta}{}^{\mathrm{T}}\boldsymbol{N}_{\beta}\left|\boldsymbol{J}\right|\mathrm{d}\xi\mathrm{d}\eta \tag{9-116}$$

When the stacking sequences of a laminated composite plate is symmetrical with respect to the mid-plane, there will be no coupling existing between the bending actions and in-plane actions. So, if only the transverse vibration is considered, $\boldsymbol{m}_{0}^{e}$ in Eq. (9-114) can be omitted. Thus, the element mass matrix can be rewritten as:

$$\boldsymbol{m}^{e}=\boldsymbol{m}_{w}{}^{e}+\boldsymbol{m}_{\beta}{}^{e} \tag{9-117}$$

After the element stiffness matrix $\boldsymbol{K}^e$ and mass matrix $\boldsymbol{m}^e$ are obtained, the vibration analysis of the plate can be performed by the usual procedure, and the natural frequency ω_i can be solved by the following generalized characteristic equation:

$$(\boldsymbol{K} - \omega^2 \boldsymbol{m})\boldsymbol{q} = \boldsymbol{0} \tag{9-118}$$

where $\boldsymbol{K}$ is the global stiffness matrix; $\boldsymbol{m}$ is the global mass matrix; $\boldsymbol{q}$ is the global nodal displacement vector.

9.6 Numerical Examples

When dealing with a single layer isotropic plate, the element CTMQ20 will degenerate into the Mindlin plate element ARS-Q12 presented in reference [25]. Good overall results were obtained for displacements, internal forces and stresses. The focus of this section is only on the composite plates.

Example 9.1 Simply supported square symmetric cross-ply laminated plate with 3 (0/90/0) or 9 (0/90/0/90/0/90/0/90/0) layers subjected to a doubly sinusoidal load.

This example, proposed by Pagano and Hatfield[29], is presented in Fig. 9.7. Each layer is strongly orthotropic and two stacking sequences are studied: ST1 corresponds to 3 layers (0/90/0) whereas ST2 corresponds to 9 layers (0/90/0/90/0/90/0/90/0). In both cases, the total thickness of all the 0° layers is the

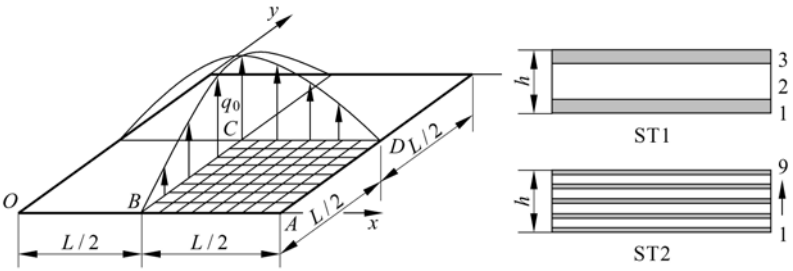

GEOMETRY
L=1000; h=250, 100, 20, 10, 1, 0.1
MATERIAL (orthotropic)
Skins: E_1=25.0; E_2=1.0; G_{12}=0.5; G_{13}=0.5; G_{23}=0.2; μ_{12}=0.25
ST1:0/90/0 symmetric
ST2:0/90/0/90/0/90/0/90/0 symmetric
BOUNDARY CONDITIONS (simply-supported: hard support mode Ⅰ)
on AB: $u=w=\psi_x=0$; on BC: $u=\psi_x=0$
on CD: $v=\psi_y=0$; on DA: $v=w=\psi_y=0$
LOADING (doubly sinusoidal)

$$q = q_0 \sin\frac{\pi x}{L}\sin\frac{\pi y}{L}$$

Figure 9.7 Square plate with 3 and 9 layers subjected to doubly sinusoidal load

same as that of all the 90° layers; and those layers having the same orientation have the same thickness. Three different meshes, i.e., 4×4, 8×8 and 16×16, are used to model a quadrant of the plate, and five *L/t* aspect ratios are considered. The correction factors can be obtained from reference [14] or [15]: $k_1^2=0.5952$, $k_2^2=0.7205$ for ST1 and $k_1^2=0.689$, $k_2^2=0.611$ for ST2.

For comparing with analytical solutions and solutions in other references, deflection and stresses are given in the form:

$$\text{Deflection:}\quad \tilde{w}=\frac{w\pi^4\hat{Q}}{12S^4hq_0}\quad\text{with}\quad S=\frac{L}{h},\quad \hat{Q}=4G_{12}+\frac{[E_1+E_2(1+2\mu_{23})]}{(1-\mu_{12}\mu_{21})}$$

(Note: $\mu_{23}=0.25$ here. It is necessary for the 3D elastic solution, but it is not needed for FDST)

$$\text{In-plane stresses:}\quad (\tilde{\sigma}_x,\tilde{\sigma}_y,\tilde{\tau}_{xy})=\frac{1}{q_0S^2}(\sigma_x,\sigma_y,\tau_{xy})$$

$$\text{Transverse shear stresses:}\quad (\tilde{\tau}_{xz},\tilde{\tau}_{yz})=\frac{1}{q_0S}(\tau_{xz},\tau_{yz})$$

Some results of the element CTMQ20 obtained together with some other solutions are presented in Tables 9.1 and 9.2, and the distributions of selective normal and transverse shear stresses along the thickness obtained by 8×8 mesh are plotted in Figs. 9.8 to 9.15.

Table 9.1 Maximum deflection and stresses in 3-ply (0/90/0) square laminate composite plate (hard simply-supported mode Ⅰ) subjected to doubly sinusoidal load

$S=L/h$	Mesh & models	$\tilde{w}$ $\left(\frac{L}{2},\frac{L}{2},0\right)$	$\tilde{\sigma}_x$ $\left(\frac{L}{2},\frac{L}{2},\pm\frac{h}{2}\right)$	$\tilde{\sigma}_y$ $\left(\frac{L}{2},\frac{L}{2},\pm\frac{h}{4}\right)$	$\tilde{\tau}_{xy}$ $\left(0,0,\pm\frac{h}{2}\right)$	$\tilde{\tau}_{xz}$ $\left(0,\frac{L}{2},0\right)$	$\tilde{\tau}_{yz}$ $\left(\frac{L}{2},0,0\right)$
4	4×4	4.888	± 0.374	± 0.674	∓ 0.0330	0.245	0.331
	CTMQ20 8×8	4.856	± 0.371	± 0.664	∓ 0.0333	0.247	0.334
	16×16	4.848	± 0.370	± 0.661	∓ 0.0334	0.248	0.335
	DST 10×10[30]	4.490	± 0.518	± 0.296		0.202	0.422
	FSDT	4.845	± 0.370	± 0.661	∓ 0.0334	0.249	0.319
10	4×4	1.735	± 0.488	± 0.407	∓ 0.0250	0.304	0.204
	CTMQ20 8×8	1.729	± 0.484	± 0.401	∓ 0.0252	0.307	0.207
	16×16	1.728	± 0.483	± 0.399	∓ 0.0253	0.308	0.208
	DST 10×10[30]	1.727	± 0.549	± 0.253		0.213	0.409
	REC56-Z0 2×2[19]	1.445	± 0.529	± 0.363	∓ 0.0250		
	REC72-Z0 2×2[19]	1.663	± 0.583	± 0.408	∓ 0.0290		
	3D elasticity[29]	1.709	± 0.559	0.401/−0.403	−0.0275/0.0276	0.301	0.196
	FSDT	1.727	± 0.483	± 0.399	∓ 0.0253	0.310	0.198

(Continued)

$S=L/h$	Mesh & models	$\tilde{w}\left(\frac{L}{2},\frac{L}{2},0\right)$	$\tilde{\sigma}_x\left(\frac{L}{2},\frac{L}{2},\pm\frac{h}{2}\right)$	$\tilde{\sigma}_y\left(\frac{L}{2},\frac{L}{2},\pm\frac{h}{4}\right)$	$\tilde{\tau}_{xy}\left(0,0,\pm\frac{h}{2}\right)$	$\tilde{\tau}_{xz}\left(0,\frac{L}{2},0\right)$	$\tilde{\tau}_{yz}\left(\frac{L}{2},0,0\right)$
50	4 × 4	1.031	± 0.543	± 0.280	∓ 0.0212	0.330	0.135
	CTMQ20 8 × 8	1.031	± 0.538	± 0.277	∓ 0.0214	0.335	0.142
	16 × 16	1.031	± 0.536	± 0.276	∓ 0.0215	0.336	0.146
	DST 10 × 10[30]	1.067	± 0.494	± 0.331		0.160	0.436
	REC56-Z0 2 × 2[19]	0.993	± 0.535	± 0.261	∓ 0.0226		
	REC72-Z0 2 × 2[19]	1.006	± 0.537	± 0.265	∓ 0.0230		
	3D elasticity[29]	1.031	± 0.539	± 0.276	∓ 0.0216	0.337	0.141
	FSDT	1.031	± 0.536	± 0.276	∓ 0.0215	0.338	0.141
100	4 × 4	1.007	± 0.545	± 0.274	∓ 0.0210	0.329	0.130
	CTMQ20 8 × 8	1.008	± 0.540	± 0.272	∓ 0.0213	0.335	0.134
	16 × 16	1.008	± 0.538	± 0.271	∓ 0.0213	0.337	0.140
	REC56-Z0 2 × 2[19]	0.956	± 0.506	± 0.248	∓ 0.0223		
	REC72-Z0 2 × 2[19]	0.962	± 0.509	± 0.249	∓ 0.0225		
	3D elasticity [29]	1.008	± 0.539	± 0.271	∓ 0.0214	0.339	0.139
	FSDT	1.008	± 0.538	± 0.271	∓ 0.0213	0.339	0.139
100 000	4 × 4	1.000	± 0.545	± 0.273	∓ 0.0210	0.326	0.128
	CTMQ20 8 × 8	1.000	± 0.540	± 0.270	∓ 0.0212	0.330	0.129
	16 × 16	1.000	± 0.539	± 0.270	∓ 0.0213	0.331	0.130
	FSDT	1.000	± 0.539	± 0.269	∓ 0.0213	0.339	0.138
	CLT[31]	1.000	± 0.539	± 0.269	∓ 0.0213	0.339	0.138

Table 9.2 Maximum deflection and stresses in 9-ply (0/90/0/90/0/90/0/90/0) square laminate composite plate (hard simply-supported mode Ⅰ) subjected to doubly sinusoidal load

$S=L/h$	Mesh & models	$\tilde{w}\left(\frac{L}{2},\frac{L}{2},0\right)$	$\tilde{\sigma}_x\left(\frac{L}{2},\frac{L}{2},\pm\frac{h}{2}\right)$	$\tilde{\sigma}_y\left(\frac{L}{2},\frac{L}{2},\pm\frac{2h}{5}\right)$	$\tilde{\tau}_{xy}\left(0,0,\frac{h}{2}\right)$	$\tilde{\tau}_{xz}\left(0,\frac{L}{2},0\right)$	$\tilde{\tau}_{yz}\left(\frac{L}{2},0,0\right)$
4	4 × 4	4.283	± 0.498	± 0.494	∓ 0.0214	0.234	0.243
	CTMQ20 8 × 8	4.252	± 0.493	± 0.489	∓ 0.0217	0.237	0.245
	16 × 16	4.244	± 0.492	± 0.487	∓ 0.0217	0.237	0.246
	DST 10 × 10[30]	4.242	± 0.547	± 0.419		0.225	0.231
	FSDT	4.242	± 0.491	± 0.487	∓ 0.0217	0.238	0.245
10	4 × 4	1.529	± 0.526	± 0.461	∓ 0.0212	0.246	0.228
	CTMQ20 8 × 8	1.524	± 0.521	± 0.456	∓ 0.0214	0.249	0.230
	16 × 16	1.523	± 0.519	± 0.455	∓ 0.0214	0.249	0.231
	DST 10 × 10[30]	1.526	± 0.541	± 0.425		0.219	0.257
	LPL-20β 8 × 8[21]	①	± 0.520	± 0.458	∓ 0.0216	0.248	0.228
	3D elasticity[29]	1.512	± 0.551	± 0.477	∓ 0.0233	0.247	0.226
	FSDT	1.522	± 0.519	± 0.454	∓ 0.0215	0.250	0.230

(Continued)

$S=L/h$	Mesh & models	$\tilde{w}\left(\frac{L}{2},\frac{L}{2},0\right)$	$\tilde{\sigma}_x\left(\frac{L}{2},\frac{L}{2},\pm\frac{h}{2}\right)$	$\tilde{\sigma}_y\left(\frac{L}{2},\frac{L}{2},\pm\frac{2h}{5}\right)$	$\tilde{\tau}_{xy}\left(0,0,\frac{h}{2}\right)$	$\tilde{\tau}_{xz}\left(0,\frac{L}{2},0\right)$	$\tilde{\tau}_{yz}\left(\frac{L}{2},0,0\right)$
50	4 × 4	1.021	± 0.545	± 0.438	∓ 0.0210	0.251	0.213
	CTMQ20 8 × 8	1.021	± 0.539	± 0.434	∓ 0.0212	0.256	0.218
	16 × 16	1.021	± 0.538	± 0.433	∓ 0.0213	0.257	0.220
	DST 10 × 10[30]	1.020	± 0.522	± 0.447		0.190	0.263
	LPL-20β 8×8[21]	①	± 0.540	± 0.434	∓ 0.0214	0.256	0.217
	3D elasticity[29]	1.021	± 0.539	± 0.433	∓ 0.0214	0.258	0.219
	FSDT	1.021	± 0.538	± 0.432	∓ 0.0213	0.258	0.219
100	4 × 4	1.005	± 0.545	± 0.437	∓ 0.0209	0.249	0.210
	CTMQ20 8 × 8	1.005	± 0.540	± 0.433	∓ 0.0212	0.254	0.215
	16 × 16	1.005	± 0.539	± 0.432	∓ 0.0213	0.257	0.218
	LPL-20β 8 × 8[21]	①	± 0.541	± 0.433	∓ 0.0214	0.257	0.217
	3D elasticity[29]	1.005	± 0.539	± 0.431	∓ 0.0213	0.259	0.219
	FSDT	1.005	± 0.538	± 0.431	∓ 0.0213	0.259	0.219
100 000	4 × 4	1.000	± 0.545	± 0.436	∓ 0.0210	0.247	0.207
	CTMQ20 8 × 8	1.000	± 0.540	± 0.432	∓ 0.0212	0.250	0.210
	16 × 16	1.000	± 0.539	± 0.431	∓ 0.0213	0.250	0.210
	FSDT	1.000	± 0.539	± 0.431	∓ 0.0213	0.259	0.219
	CLT[31]	1.000	± 0.539	± 0.431	∓ 0.0213	0.259	0.219

① Reference [21] pointed out that the computational error of the deflection by the element LPL-20β is big, so the results were not given.

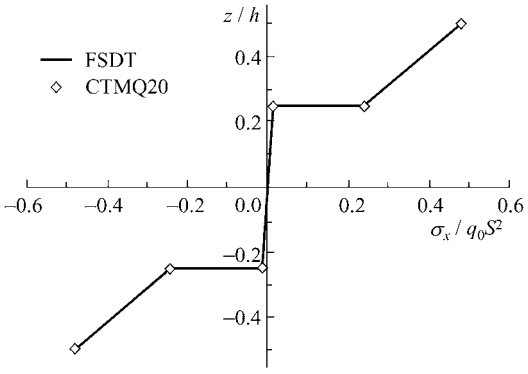

Figure 9.8 The distribution of central stress σ_x along thickness for a square 3-ply plate (doubly sinusoidal load, $L/h = 10$, 8×8 mesh)

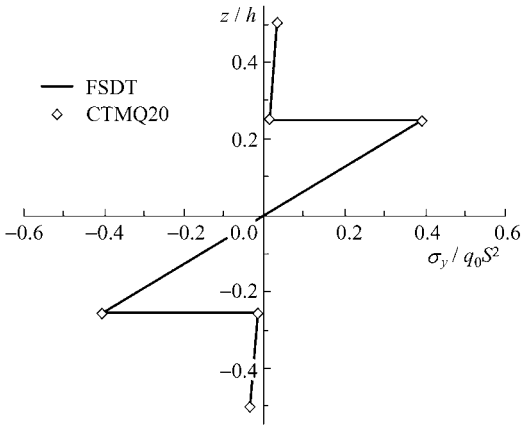

Figure 9.9 The distribution of central stress σ_y along thickness for a square 3-ply plate (doubly sinusoidal load, $L/h = 10$, 8×8 mesh)

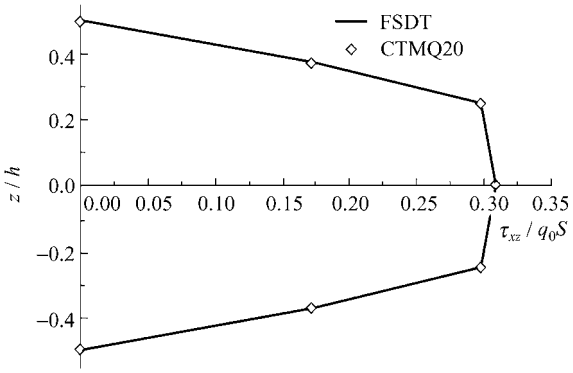

Figure 9.10 The distribution of τ_{xz} at (0, L/2) along thickness of a square 3-ply plate (doubly sinusoidal load, $L/h = 10$, 8×8 mesh)

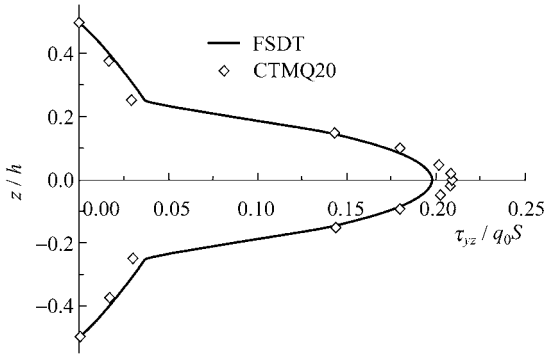

Figure 9.11 The distribution of τ_{yz} at (L/2, 0) along thickness of a square 3-ply plate (doubly sinusoidal load, $L/h = 10$, 8×8 mesh)

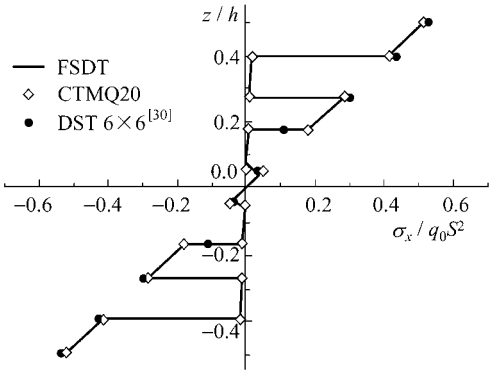

Figure 9.12 The distribution of central stress σ_x along thickness for a square 9-ply plate (doubly sinusoidal load, $L/h = 10$, 8×8 mesh)

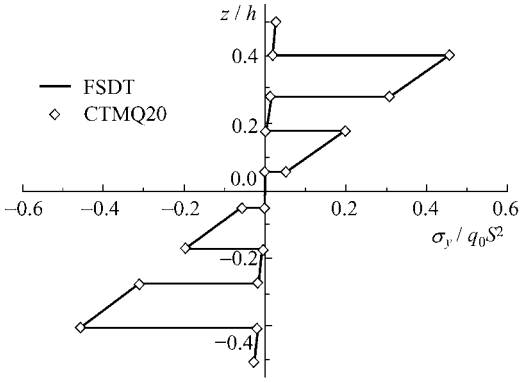

Figure 9.13 The distribution of central stress σ_y along thickness for a square 9-ply plate (doubly sinusoidal load, $L/h = 10$, 8×8 mesh)

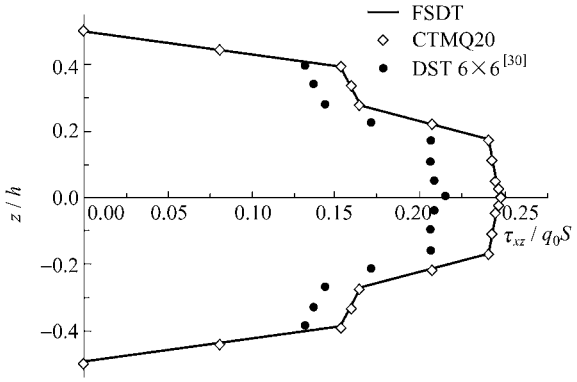

Figure 9.14 The distribution of τ_{xz} at (0, L/2) along thickness of a square 9-ply plate (doubly sinusoidal load, $L/h = 10$, 8×8 mesh)

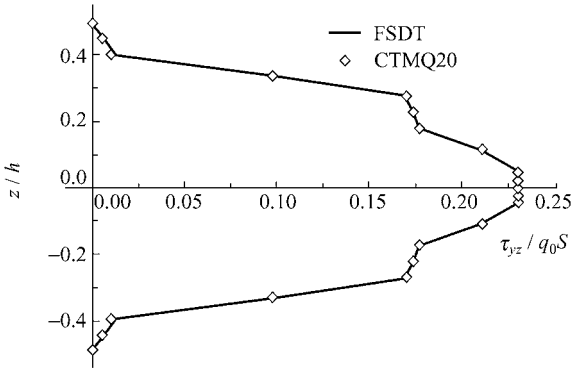

Figure 9.15 The distribution of τ_{yz} at (L/2, 0) along thickness of a square 9-ply plate (doubly sinusoidal load, $L/h = 10$, 8×8 mesh)

With regards to the central deflection w_C and maximum plane stresses σ_x, σ_y and τ_{xy}, the results obtained using the CTMQ20 element are in excellent agreement with those of the exact FSDT for all span-thickness ratio L/t. No shear locking happens in the thin plate limit. The results obtained using three different meshes show rapid convergence for the above-mentioned deflection and stresses. For transverse shear stresses, the element CTMQ20 can still produces good results, which the usual displacement-based element cannot do.

It is obvious that the performance of the element CTMQ20 is much better than those obtained using the quadrilateral hybrid element LPL-20β by Wu et al.[21], the element DST (a discrete shear triangular plate-bending element) by Lardeur et al.[30], REC56-Z0 (56 DOFs per element) and REC72-Z0 (72 DOFs per element) by Sadek[19].

Example 9.2 Simply supported (hard support mode Ⅱ) anti-symmetric angle-ply square plate with 2 $(-45/45)$ or 8 $[(-45/45)_4]_s$ layers subjected to doubly sinusoidal load.

The geometry, the material constants and the loading are the same as those given in Example 9.1. All the layers have the same thickness. The boundary conditions (hard simply-supported mode Ⅱ) are:

$$\text{at } x = 0 \text{ and } x = L\text{: } u = w = \psi_y = 0\text{; at } y = 0 \text{ and } y = L,\ v = w = \psi_x = 0.$$

Six different meshes, i.e., 4×4, 8×8, 16×16, 32×32, 64×64 and 80×80, are used to model the whole plate and three L/h aspect ratios are considered. For comparison with the analytical solution in reference [1], the shear correction factors are taken as: $k_1^2 = k_2^2 = 5/6$. The results are shown in Tables 9.3 and 9.4. It can be seen that excellent solutions for deflection and in-plane stresses can be obtained from the element CTMQ20. For the anti-symmetric or unsymmetric cases, most of the simple displacement-based elements cannot produce good results for the transverse shear stresses using the equilibrium equation[18]. Since

Table 9.3 Maximum deflection and stresses in 2-ply (– 45/45) square laminate composite plate (hard simply-supported mode Ⅱ) subjected to doubly sinusoidal load

L/h	Model & mesh		$w(L/2, L/2)\times 100E_2h^3/(L^4q_0)$	$\sigma_x(L/2, L/2, h/2)\times h^2/(L^2q_0)$	$\tau_{xy}(0, 0, -h/2)\times h^2/(L^2q_0)$	$\tau_{xz}(0, L/2, h/4)\times h/(Lq_0)$
10	CTMQ20	4 × 4	0.8042	0.2628	0.2291	0.1683
		8 × 8	0.8218	0.2543	0.2349	0.2005
		16 × 16	0.8267	0.2510	0.2341	0.2107
		32 × 32	0.8280	0.2501	0.2337	0.2134
		64 × 64	0.8283	0.2499	0.2336	0.2141
		80 × 80	0.8283	0.2498	0.2336	0.2142
	FSDT[1]		0.8284	0.2498	0.2336	0.2143
20	CTMQ20	4 × 4	0.6733	0.2501	0.2211	0.1324
		8 × 8	0.6906	0.2523	0.2333	0.1773
		16 × 16	0.6961	0.2508	0.2339	0.2027
		32 × 32	0.6976	0.2501	0.2337	0.2112
		64 × 64	0.6980	0.2499	0.2336	0.2136
		80 × 80	0.6980	0.2498	0.2336	0.2138
	FSDT[1]		0.6981	0.2498	0.2336	0.2143
100	CTMQ20	4 × 4	0.6399	0.2399	0.2157	0.1049
		8 × 8	0.6519	0.2474	0.2295	0.1194
		16 × 16	0.6550	0.2495	0.2328	0.1362
		32 × 32	0.6560	0.2499	0.2335	0.1691
		64 × 64	0.6563	0.2499	0.2336	0.1980
		80 × 80	0.6564	0.2498	0.2336	0.2033
	FSDT[1]		0.6564	0.2498	0.2336	0.2143

Table 9.4 Maximum deflection and stresses in 8-ply $[(-45/45)_4]_s$ square laminate composite plate (hard simply-supported mode Ⅱ) subjected to doubly sinusoidal load

L/h	Model & mesh		$w(L/2, L/2)\times 100E_2h^3/(L^4q_0)$	$\sigma_x(L/2, L/2, h/2)\times h^2/(L^2q_0)$	$\tau_{xy}(0, 0, -h/2)\times h^2/(L^2q_0)$	$\tau_{xz}(0, L/2, 0)\times h/(Lq_0)$
10	CTMQ20	4 × 4	0.4063	0.1657	0.1268	0.2131
		8 × 8	0.4157	0.1507	0.1361	0.2384
		16 × 16	0.4188	0.1461	0.1379	0.2460
		32 × 32	0.4196	0.1449	0.1383	0.2480
		64 × 64	0.4198	0.1446	0.1384	0.2485
		80 × 80	0.4198	0.1446	0.1384	0.2486
	FSDT[1]		0.4198	0.1445	0.1384	0.2487
20	CTMQ20	4 × 4	0.2764	0.1575	0.1223	0.1850
		8 × 8	0.2846	0.1496	0.1353	0.2225
		16 × 16	0.2881	0.1460	0.1378	0.2408
		32 × 32	0.2892	0.1449	0.1383	0.2466
		64 × 64	0.2895	0.1446	0.1384	0.2481
		80 × 80	0.2895	0.1446	0.1384	0.2483
	FSDT[1]		0.2896	0.1445	0.1384	0.2487
100	CTMQ20	4 × 4	0.2440	0.1499	0.1283	0.1674
		8 × 8	0.2463	0.1459	0.1356	0.1791
		16 × 16	0.2471	0.1451	0.1374	0.1904
		32 × 32	0.2476	0.1448	0.1380	0.2172
		64 × 64	0.2478	0.1446	0.1383	0.2380
		80 × 80	0.2478	0.1446	0.1383	0.2416
	FSDT[1]		0.2479	0.1445	0.1384	0.2487

the hybrid-enhanced post-processing procedure is used by the present element, it is obvious that good results of transverse shear stresses can be obtained.

Example 9.3 Free vibration analysis of a 3-ply (0/90/0) square plate (hard simply-supported mode Ⅰ).

All the layers have the same thickness. Other geometry, the material constants, the load and the boundary conditions are the same as those given in Example 9.1. A 16×16 mesh is used for the whole plate and two span-thickness ratios are considered. For comparison with the analytical solution in reference [1], the shear correction factors are taken as: $k_1^2=k_2^2=1$. The first seven dimensionless natural frequencies obtained are listed in Table 9.5. It can be seen that the element CTMQ20 can provide accurate results.

Table 9.5 The free frequency coefficients $\tilde{\omega}=\omega(L^2/h)\sqrt{\rho/E_2}$ for a 3-ply (0/90/0) square laminate composite plate (hard simply-supported mode Ⅰ)

L/h	Mode *m* in *x*-direction	Mode *n* in *y*-direction	CLT[1]	FSDT[1]	CTMQ20 $16\times16$①
10	1	1	15.104	12.527	12.464 (– 0.50%)
	1	2	22.421	19.203	18.974 (– 1.19%)
	1	3	38.738	31.921	31.377 (– 1.70%)
	2	1	55.751	32.931	32.641 (– 0.88%)
	2	2	59.001	36.362	35.641 (– 1.98%)
	1	4	62.526	44.720	43.350 (– 3.06%)
	2	3	67.980	47.854	46.722 (– 2.36%)
100	1	1	15.227	15.191	15.142 (– 0.32%)
	1	2	22.873	22.827	22.659 (– 0.74%)
	1	3	40.283	40.174	39.871 (– 0.75%)
	2	1	56.874	56.319	56.123 (– 0.35%)
	2	2	60.891	60.322	59.556 (– 1.27%)
	1	4	66.708	66.421	65.939 (– 0.73%)
	2	3	71.484	70.764	69.244 (– 2.14%)

① The numbers in parentheses are percentage errors.

Example 9.4 Free vibration analysis of anti-symmetric angle-ply square plates (hard simply-supported mode Ⅱ) with 2 (– 45/45) and 8 $[(-45/45)_4]_s$ layers.

All the layers have the same thickness. Boundary conditions are the same as those given in Example 9.2. There are two material cases:

Material 1: $E_1=25.0$; $E_2=1.0$; $G_{12}=0.5$; $G_{13}=0.5$; $G_{23}=0.2$; $\mu_{12}=0.25$

Material 2: $E_1=40.0$; $E_2=1.0$; $G_{12}=0.6$; $G_{13}=0.6$; $G_{23}=0.5$; $\mu_{12}=0.25$

A 16×16 mesh is used for the whole plate, and four span-thickness ratios are considered. For comparison with the analytical solution in reference [1], the shear

correction factors are taken as: $k_1^2 = k_2^2 = 5/6$. The results of the first natural frequency are listed in Table 9.6.

Table 9.6 The first natural frequency coefficients $\tilde{\omega} = \omega(L^2/h)\sqrt{\rho/E_2}$ for anti-symmetric angle-ply square laminate composite plate (hard simply-supported mode Ⅱ)

L/h		Material 1		Material 2	
		2-ply (−45/45)	8-ply $[(-45/45)_4]_s$	2-ply (−45/45)	8-ply $[(-45/45)_4]_s$
5	CTMQ20	8.457	10.244	10.285	12.842
	16×16	(−0.48%)	(−0.40%)	(−4.76%)	(−0.40%)
	FSDT[1]	8.498	10.285	10.799	12.893
10	CTMQ20	10.860	15.349	13.002	19.242
	16×16	(−0.32%)	(−0.25%)	(−4.60%)	(−0.24%)
	FSDT[1]	10.895	15.388	13.629	19.289
20	CTMQ20	11.908	18.535	14.149	23.237
	16×16	(−0.21%)	(−0.11%)	(−4.50%)	(−0.09%)
	FSDT[1]	11.933	18.555	14.815	23.259
100	CTMQ20	12.315	20.049	14.581	25.134
	16×16	(−0.21%)	(−0.17%)	(−4.54%)	(−0.17%)
	FSDT[1]	12.341	20.084	15.274	25.176

Note: The numbers in parentheses are percentage errors.

References

[1] Reddy JN (1997) Mechanics of laminated composite plates—theory and analysis. CRC Press, Boca Raton

[2] Calcote LR (1969) The analysis of laminated composite structures. Van Nostrand Reinhold, New York

[3] Jones RM (1975) Mechanics of composite material. MacGraw-Hill Kogakusha, Tokyo

[4] Medwadowski SJ (1958) A refined theory of elastic orthotropic plates. ASME J Appl Mech, 25: 437 – 443

[5] Yang PC, Norris CH, Stavsky Y (1966) Elastic wave propagation in heterogeneous plates. International Journal of Solids and Structures 2: 665 – 684

[6] Lo KH, Christensen RM, Wu EM (1977) A higher-order theory of plate deformation, Part Ⅱ: Laminated plates. Journal of Applied Methanics 44(4): 663 – 668

[7] Reddy JN (1984) A simple higher-order theory for laminated composite plates. Journal of Applied Methanics 51: 745 – 752

[8] Phan ND, Reddy JN (1985) Analysis of laminated composite plates using a higher-order shear deformation theory. International Journal for Numerical Methods in Engineering 21: 2201 – 2219

[9] Pandya BN, Kant T (1988) Flexural analysis of laminated composites using refined higher-order C^0 plate bending elements. Computer Methods in Applied Mechanics and Engineering 66: 173 – 198

[10] Kant T, Owen DRJ, Zienkiewicz OC (1982) A refined higher-order C^0 plate bending element. Computers & Structures 15: 177 – 183

[11] Reddy JN (1987) A generalization of two-dimensional theories of laminated composite plates. Communications in Applied Numerical Methods 3: 173 – 180

[12] Robbins DH, Reddy JN (1993) Modelling of thick composites using a layerwise laminate theory. International Journal for Numerical Methods in Engineering 36: 655 – 677

[13] Pryor CW, Barker RM (1971) A finite element analysis including transverse shear effects for application to laminated plates. AIAA Journal 9: 912 – 917

[14] Vlachoutsis S (1992) Shear correction factors for plates and shells. International Journal for Numerical Methods in Engineering 33: 1537 – 1552

[15] Auricchio F, Sacco E (199) A mixed-enhanced finite-element for the analysis of laminated composite plates. International Journal for Numerical Methods in Engineering 44: 1481 – 1504

[16] Rolfes R, Rohwer K (1997) Improved transverse shear stresses in composite finite elements based on first order shear deformation theory. International Journal for Numerical Methods in Engineering 40: 51 – 60

[17] Rolfes R, Rohwer K, Ballerstaedt M (1998) Efficient linear transverse normal stress analysis of layered composite plates. Computers & Structures 68: 643 – 652

[18] Singh G, Raju KK, Rao GV (1998) A new lock-free, material finite element for flexure of moderately thick rectangular composite plates. Computers & Structures 69: 609 – 623

[19] Sadek EA (1998) Some serendipity finite element for the analysis of laminated plates. Computers & Structures 69: 37 – 51

[20] Alfano G, Auricchio F, Rosati L, Sacco E (2001) MITC finite elements for laminated composite plates. International Journal for Numerical Methods in Engineering 50: 707 – 738

[21] Wu CC, Pian THH (1997) Incompatible Numerical Analysis and Hybrid Finite Element Method. Beijing: Science Press (in Chinese)

[22] Cen S, Long YQ, Yao ZH (2002) A new element based on the first-order shear deformation theory for the analysis of laminated composite plates. Gong Cheng Li Xue/Engineering Mechanics 19(1): 1 – 8 (in Chinese)

[23] Cen S, Long YQ, Yao ZH (2002) A new hybrid-enhanced displacement-based element for the analysis of laminated composite plates. Computers & Structures 80 (9-10): 819 – 833

[24] Cen S, Long ZF, Long YQ (1999) A Mindlin quadrilateral plate element with improved interpolation for the rotation and shear strain fields. Gong Cheng Li Xue/Engineering Mechanics 16(4): 1 – 15 (in Chinese)

[25] Soh AK, Cen S, Long YQ, Long ZF (2001) A new twelve DOF quadrilateral element for analysis of thick and thin plates. European Journal of Mechanics A/Solids 20: 299 – 326

[26] Cen S, Long YQ, Yao ZH (2001) An enhanced hybrid post-processing procedure for improving stress solutions of displacement-based plate bending elements. Gong Cheng Li Xue/Engineering Mechanics 18(3): 21 – 27 (in Chinese)

[27] Ayad R, Dhatt G, Batoz JL (1998) A new hybrid-mixed variational approach for Reissner-Mindlin plates: The MiSP model. International Journal for Numerical Methods in Engineering 42:1149 – 1179

[28] Pian THH, Sumihara K (1984) Rational approach for assumed stress finite element. International Journal for Numerical Methods in Engineering 20: 1685 – 1695

[29] Pagano NJ, Hatfield SJ (1972) Elastic behavior of multilayered bidirectional composites. AIAA Journal 10: 931 – 933

[30] Lardeur P, Batoz JL (1989) Composite plate analysis using a new discrete shear triangular finite element. International Journal for Numerical Methods in Engineering 27: 343 – 359

[31] Pagano NJ (1970) Exact solutions for rectangular bidirectional composites and sandwich plates. J Compos Mater 4: 20 – 34